

# Palaeomagnetism from multi-orogenic terranes is ‘not a simple game’: Pyrenees’ Palaeozoic warning

Daniel Pastor-Galán<sup>1,2,3</sup> Oscar Groenhof,<sup>4</sup> Emilio L. Pueyo,<sup>5</sup> Esther Izquierdo-Llavall,<sup>6</sup> Jaume Dinarès-Turell<sup>1,7</sup> and Mark J. Dekkers<sup>4</sup>

<sup>1</sup>Frontier Research Institute for Interdisciplinary Science, Tohoku University, Sendai, Miyagi 980-8577, Japan. E-mail: [dpastorgalan@gmail.com](mailto:dpastorgalan@gmail.com)

<sup>2</sup>Center for North East Asian Studies, Tohoku University, 980-8576, 41 Kawauchi, Aoba-ku, Sendai, Miyagi 980-8577, Japan

<sup>3</sup>Department Earth Science, Tohoku University, Sendai, Miyagi 980-8577, Japan

<sup>4</sup>Paleomagnetic Laboratory ‘Fort Hoofddijk’, Utrecht University, 3584 CS Utrecht, The Netherlands

<sup>5</sup>Instituto Geológico y Minero de España (CN IGME-CSIC), Unidad de Zaragoza, 50009 Zaragoza, Spain

<sup>6</sup>Université de Pau et des Pays de l’Adour, E2S UPPA, CNRS, TOTAL, LFCR, Pau, Avenue de l’Université, 64000 Pau, France

<sup>7</sup>Istituto Nazionale di Geofisica e Vulcanologia, Via di Vigna Murata, 605, 00143 Rome, Italy

Accepted 2021 June 23. Received 2021 June 20; in original form 2021 March 16

## SUMMARY

Palaeomagnetism is a versatile tool in the Earth sciences: it provides critical input to geological timescales and plate tectonic reconstructions. Despite its undeniable perks, palaeomagnetism is not without complications. Remagnetizations overprinting the original magnetic signature of rocks are frequent, especially in orogens which tend to be the areas with better rock exposure. Unraveling the magnetic history of the rocks is a complicated task, especially in areas that underwent several orogenic pulses. In turn, constraining the timing of remagnetization represents an opportunity to solve post-magnetization structural and tectonic kinematics. Here, we evaluate the magnetization history of Silurian-Devonian carbonates from the Axial Zone of the Pyrenees. The Pyrenees are a multi-orogenic mountain belt where Silurian-Devonian rocks have seen the Variscan collision (late Palaeozoic), the opening of the Atlantic/Bay of Biscay (early Cretaceous) and the Alpine orogeny (late Cretaceous to Miocene). Our results show widespread remagnetization(s) carried by magnetite and pyrrhotite in the Silurian-Devonian series of the Pyrenees. The majority of the samples show a post-folding but pre-alpine tilting magnetization. Considering the equatorial inclinations found in such samples, we suggest that they likely acquired their magnetization during the late Carboniferous and early Permian times. Two of the studied sites (located at the western Axial Zone) were subsequently remagnetized at the end of the Alpine orogeny. The palaeomagnetic results constrained that the Variscan orogeny was responsible for the main folding event affecting Palaeozoic rocks in the Axial Zone, whereas the Alpine orogeny produced the large-scale thrusting and antiformal stacking of these units. In addition, we observed a general clockwise rotational pattern which could be related with the formation of the Cantabrian Orocline and/or rotations associated with the Alpine orogeny. The Silurian-Devonian carbonates are thus useful to understand the tectonic evolution of the Pyrenean mountain range after a systematic combination of palaeomagnetism with structural and petrological observations. In contrast, the secondary character of magnetization and complications associated with the Variscan tectonics indicate that a reassessment of Siluro-Devonian poles from the Variscan elsewhere in Europe might be appropriate.

**Key words:** Remagnetization.

## 1. INTRODUCTION

The Earth’s magnetic field has left a remnant signature in the geological record through eons. These magnetic signals in the rock archive have been crucial to almost any field of Earth Sciences,

from the development of plate tectonics (e.g. Vine and Matthews 1963), to the development of global timescales (e.g. Kuiper *et al.* 2008) or the origin and evolution of the core (e.g. Biggin *et al.* 2015). Palaeomagnetism is still the only available technique that can quantify pre-Jurassic palaeolatitudes (Domeier and Torsvik 2019),

intensities of the past magnetic field or global reference times through reversals. The palaeomagnetic imprint in rocks can last billions of years but may be also fragile. For example, remagnetizations that overprint or even delete the original magnetic signature are ubiquitous, especially in orogenic belts (e.g. Pueyo *et al.* 2007, Van der Voo & Torsvik 2012; 2016a; Huang *et al.* 2017). The majority of the studies associated with the preservation and reacquisition of a magnetic remanence in rocks are relatively recent. Although remagnetizations were initially recognized already during the 1960s and remarked its importance in the 1980s (McCabe *et al.* 1983; McCabe and Elmore 1989), they have been studied in particular detail only from the first two decades of the 21st century onward (*cf.* van der Voo and Torsvik 2012). Since then palaeomagnetists and rock magnetists have realized to the full that a plethora of chemical and physical processes are capable of resetting the magnetic signature in a rock (e.g. Jackson *et al.* 1993; Weil Arlo & Van der Voo ; Dekkers 2012; Pastor-Galán *et al.* 2017; Aubourg *et al.* 2019; Huang *et al.* 2020).

Remagnetization is often deemed a problem because it interferes with palaeogeographic reconstructions that rely on the analysis of primary natural remanent magnetization (NRM), that is the age of the NRM is the same as the age of the sampled rock unit. Despite the perceived loss of information, remagnetized rocks do represent valuable sources of geological information when it is possible to retrieve precisely the timing of the resetting of the original NRM acquisition, that is the remagnetization. Remagnetized rocks have been successfully used to unravel palaeolatitudes of orogenic processes, orogenic kinematics, as geothermometers, to reconstruct inverted basins, etc. (e.g. Dinares-Turell and Garcia-Senz 2000, Huang *et al.* 2015; Villalain *et al.* 2016; Aubourg *et al.* 2019; Izquierdo-Llavall *et al.* 2020). Rocks with complex orogenic histories—the rule in many orogens—present a myriad of complications including the timing of their NRM acquisition. In such settings, palaeomagnetism can be an excellent tool to understand multiphase orogenic systems (and remagnetizations helpful to observe snapshots of deformation histories) if wisely used in concert with other geological tools.

Many palaeomagnetic studies were performed before our current understanding of remagnetization processes and for a given region, time frame or lithology, those older palaeomagnetic data may be the only data available. There is an evident need to review and critically reassess such palaeomagnetic information: regional and even global geologic interpretations are still grounded in them. In this paper, we reappraise the palaeomagnetism from Silurian–Devonian limestones in the Pyrenean mountain belt, from which only three rather limited studies have been previously published (Tait *et al.* 2000; Gil-Peña *et al.* 2006; Izquierdo-Llavall *et al.* 2020). From these data sets, Tait *et al.* (2000) interpreted that the magnetic signal carried by Silurian–Devonian units was primary and subsequent plate reconstructions (e.g. Domeier & Torsvik 2014) have relied on this suggested magnetization age to create the Devonian palaeogeography of Europe, but that date might have been remagnetized or not corrected properly as witnessed by several younger studies (e.g. Izquierdo-Llavall *et al.* 2018, and references therein). Our results, together with an enhanced geologic and palaeomagnetic knowledge of the orogen, show that the sampled Silurian–Devonian carbonates were completely remagnetized during the late Carboniferous and Early Permian, when they could experience significant clockwise vertical axis rotations. These rocks were partially overprinted yet another time during Cretaceous and Cenozoic times, and experienced extension, compression, tilting and vertical axis rotations related to both the opening of the Bay of Biscay in the Late Mesozoic and the

Cenozoic building of the Alpine chain in the Pyrenees. The magnetization history of the Pyrenees is a warning for palaeomagnetists beautifully illustrated in Chris Scotese's anagram: PALAEOMAGNETISM = NOT A SIMPLE GAME (Van der Voo 1993).

## 2. THE PYRENEAN MOUNTAIN BELT

The Pyrenees are a mountainous barrier that separates the Iberian Peninsula from the rest of Eurasia. They are a prime example of the superposition of different tectonic events: (1) the multiphase late Palaeozoic Variscan orogeny; (2) the Jurassic and early Cretaceous major extension resulting into the formation of oceanic crust in the Atlantic Ocean and the Bay of Biscay and the exhumation of the mantle between the Neotethys and Atlantic Oceans along the current Pyrenees; (3) the closure of this previously opened seaway in the late Cretaceous and (4) the final collision between the Iberian and Eurasian plates during the Cenozoic (Muñoz 1992, 2019, and references therein).

### 2.1 Palaeozoic history: Variscan cycle

The tectonic evolution of the Palaeozoic era was dominated by the progressive amalgamation of most continents into Pangea (e.g. Domeier & Torsvik 2014; Domeier 2016), the latest supercontinent (Pastor-Galán *et al.* 2019a). In western Europe the Pangean amalgamation history is recorded in the Variscan orogen, which sutured the continents of Gondwana and Laurussia along with a variable number of smaller plates that likely drifted away from Gondwana (e.g. Nance *et al.* 2010). On the basis of palaeomagnetic data, Iberia has been considered part of a ribbon continent (usually named Armorica, Galatia, or Hun) that detached from Gondwana and drifted to the north or northwest in the Late Silurian or Early Devonian (e.g. van der Voo 1993; Tait *et al.* 2000; Tait 1999; Stampfli *et al.* 2013; Domeier and Torsvik 2014). Other authors, however, place Iberia along the passive margin of Gondwana throughout the Palaeozoic based on the fossil record or the provenance of detrital zircons (e.g. Robardet 2003; Pastor-Galán *et al.* 2013a). Convergence leading up to the Variscan orogen started *ca.* 420 Ma (e.g. Franke *et al.* 2017) and continued until the complete consumption of the Rheic ocean and other minor oceanic basins that existed between Gondwana and Laurussia at *ca.* 280 Ma (e.g. Pastor-Galán 2020). The final continent–continent collision was diachronic and became progressively younger westwards (in present-day coordinates) with Devonian continent–continent collision along the eastern boundary of the Variscan orogen, progressing to earliest Permian ages in the westernmost sector (e.g. Pastor-Galán *et al.* 2020, and references therein).

Iberia has the largest exposure of the Variscan orogen in Europe, and an almost continuous cross section of the orogen (e.g. Azor *et al.* 2019). The majority of the Palaeozoic outcrops in Iberia contain Gondwanan affinity rocks (e.g. Pastor-Galán *et al.* 2013a; Casas *et al.* 2019) and only a little sector of Southwest Iberia shows Laurussian affinity (e.g. Pérez-Cáceres *et al.* 2017). Geographically, the external zones of the Gondwana margin are nested to the north into the core of the Cantabrian Orocline (Fig. 1a), whereas the hinterland zones are to the west, centre and northeast of Iberia (Fig. 1a; e.g. Azor *et al.* 2019). The stratigraphy of the Gondwanan authochthon consists of Neoproterozoic arc rocks (e.g. Fernández-Suárez *et al.* 2014), which evolved to a rift-to-drift sequence during the Cambrian to early Ordovician and then to an Ordovician to late

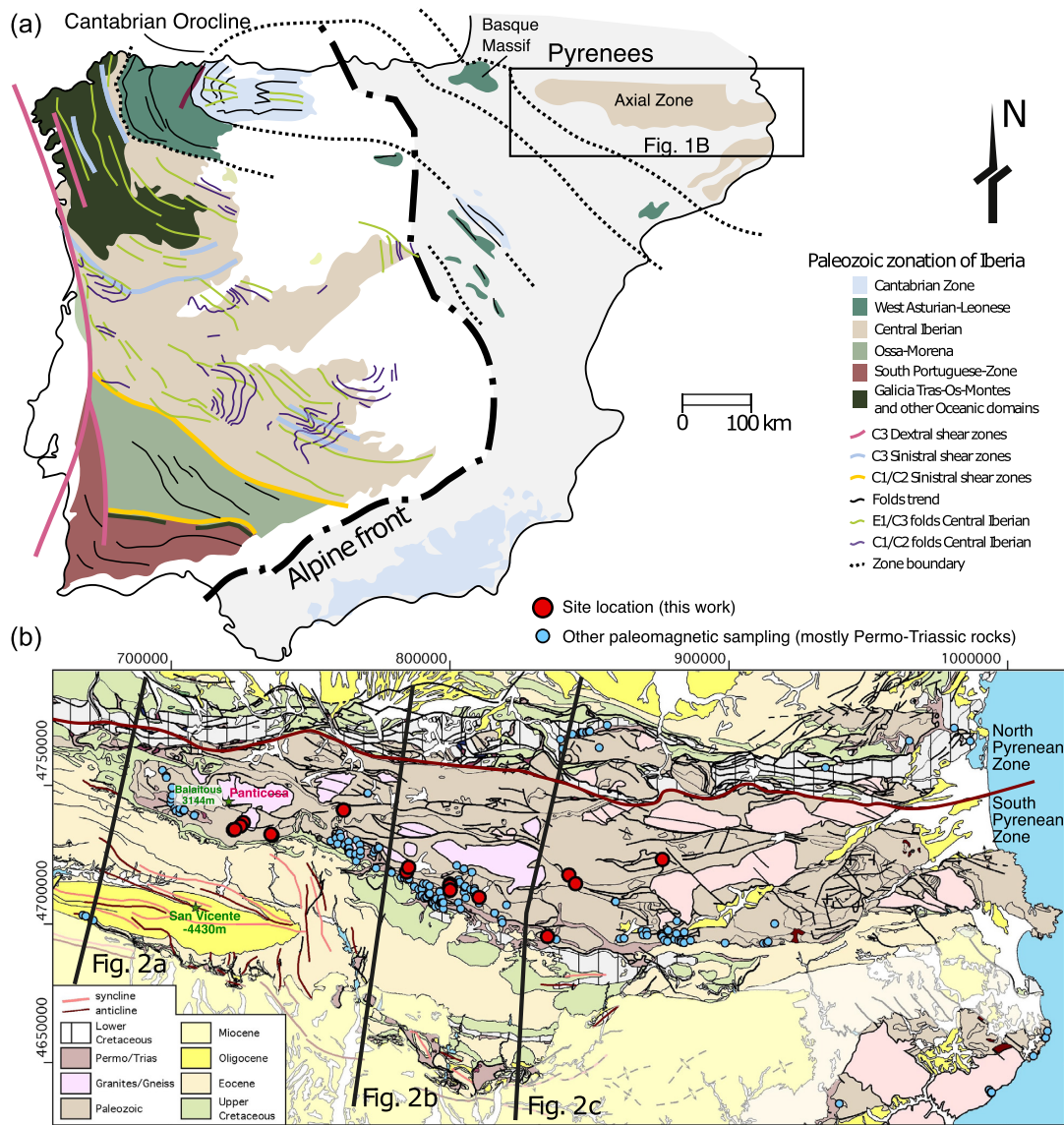


**Figure 1.** (a) Simplified map of the Iberian Peninsula showing the main Palaeozoic outcrops and the areas affected by the Alpine orogeny (after Pastor-Galán *et al.* 2020). (b) Geological map of the Pyrenees (modified from Barnolas *et al.* 2008 according to Choukroune and Séguert 1973) showing our sampling locations (red dots) and the extensive palaeomagnetic studies in the Pyrenees focused mainly on Permo-Triassic rocks (blue dots). Lines show the trend of the cross sections in Fig. 2.

Devonian passive margin basin sequence (e.g. Gutiérrez-Alonso *et al.* 2020). During the Carboniferous and early Permian, the rocks recorded up to six phases of deformation (e.g. Dias da Silva *et al.* 2020; Pastor-Galán *et al.* 2020, and references therein), metamorphism (e.g. Ribeiro *et al.* 2019) and synorogenic sedimentation processes that evolved to post-orogenic and intracontinental style basins during the Permian (e.g. Oliveira *et al.* 2019).

The trend of the Variscan belt in north Iberia follows a ‘C’ shape known as the Cantabrian Orocline (e.g. Pastor-Galán *et al.* 2020). The Cantabrian Orocline seems isoclinal, formed by a northern and a southern E–W-trending limbs, but this is likely the product of a retightening during the Alpine orogeny (e.g. Pastor-Galán *et al.* 2011; Leite Mendes *et al.* 2021; Fig. 1a). All kinematic data studied so far support a model in which the Cantabrian Orocline formed due to secondary vertical-axis rotation in a period of time later than 315 Ma and earlier than 290 Ma. Overall, the southern limb of

the orocline rotated counterclockwise (CCW) and the northern limb clockwise (CW; e.g. Weil *et al.* 2013). Orocline formation postdates the main Variscan orogenic phases (e.g. Pastor-Galán *et al.* 2015a). The development of the Cantabrian Orocline implies the existence of a roughly linear orogenic belt during the early Variscan closure of the Rheic Ocean (with an approximately N–S orientation in present-day coordinates), which was subsequently bent in map-view into an orocline during the late stages of Pangea’s amalgamation. This interpretation is grounded in extensive palaeomagnetic, structural and geochronological studies (e.g. Weil *et al.* 2001; Pastor-Galán *et al.* 2015b; Shaw *et al.* 2015; Gutiérrez-Alonso *et al.* 2015; Pastor-Galán *et al.* 2018).

The Palaeozoic rocks of the Pyrenees form the backbone of the Pyrenean chain and crop out in two areas (the Axial Zone and the Basque Massifs, to the east and west, respectively) that define an E–W elongated strip unconformably overlain by Mesozoic

and Cenozoic rocks (Figs 1a and b). These outcrops are geographically disconnected from neighboring Palaeozoic outcrops of the Catalan Coastal Range and Balearic zone to the southeast, the Mouthoumet and Montagne Noire (southern French Central massifs) to the north, Corsica–Sardinia to the east and the Iberian Massif to the west and southwest. The pre-Permian rocks of the Pyrenees recorded a polyphase deformation during the Variscan orogeny with metamorphism that ranges from absent to high grade (e.g. Casas *et al.* 2019). So far, no relics of early Variscan deformation and/or subduction related high pressure metamorphism have been found. Most palaeogeographic reconstructions suggest that the Pyrenean Palaeozoic outcrops (Fig. 1) may be equivalent to the northern branch of the Cantabrian Orocline (e.g. García-Sansegundo *et al.* 2011; Pastor-Galán *et al.* 2020). Deformation, structural style and metamorphic grade show important differences along strike in the Pyrenees (Autran and García-Sansegundo 1996; Debon and Guitard 1996) and a N–S zonation, with fold-related cleavage being pervasive in the central and northern part of the Axial Zone but poorly developed in the south (García-Sansegundo *et al.* 2011). The superposition of the later Mesozoic extension and subsequent Alpine orogeny markedly complicate an integral interpretation of the Variscan portions of the Pyrenees (see Casas *et al.* 2019). As a consequence, a comprehensive scheme integrating all the available data is lacking despite decades of geological research (e.g. de Sitter & Zwart 1957; Kleinsmiede 1960; Zwart 1979, 1986). In general terms, the Silurian, Devonian and Carboniferous successions show no to low-grade metamorphism and are composed of carbonates and shales (e.g. Casas *et al.* 2019). During the Carboniferous and Early Permian, the Pyrenees recorded an intense igneous activity including syn- to post-kinematic plutonism and volcanism (Fig. 1b; e.g. Gleizes *et al.* 1997, 2006; Denèle *et al.* 2011, 2014; Porquet *et al.* 2017), sometimes interpreted as subduction related (e.g. Pereira *et al.* 2014).

## 2.2 Mesozoic to present day evolution: Alpine cycle

The final break-up of Pangea is marked with the opening of the Central and South Atlantic from late Triassic times onward (e.g. Müller *et al.* 2019). During the Jurassic, Iberia was attached to Europe and North America as another piece of Laurasia. In the Cretaceous, the breakup and spreading in the North Atlantic led to the separation of the Iberian microplate from Eurasia, North America and Africa (e.g. Vissers & Meijer 2012). During the North Atlantic breakup, the Bay of Biscay opened, leading to approximately 35° of counter-clockwise (CCW) rotation of Iberia (Van der Voo 1969; Neres *et al.* 2013; Nierengarten *et al.* 2018) probably during the Aptian (Juárez *et al.* 1998; Gong *et al.* 2008). The opening of the Bay of Biscay to the west got recorded in the Pyrenees with the formation of a hyperextended margin with mantle exhumation during the Albian–Cenomanian (e.g. Lagabrielle *et al.* 2010). The rotation of Iberia, together with the increased convergence between Africa and Eurasia culminated in the collision between Iberia and Eurasia to form the Pyrenean range during Late Cretaceous–Miocene in the frame of the Alpine orogeny (e.g. Muñoz 2019).

Palaeozoic rocks in the Pyrenees are involved in a doubly-verging, asymmetric fold-and-thrust system with the main Alpine thrust sheets in the Axial Zone being South-verging (Muñoz 1992, 2019; Barnolas *et al.* 2019). They provoked over 100 km of N–S shortening and the southward displacement of the Palaeozoic rocks in the Axial Zone over the autochthonous basement in the southern Pyrenean foreland. The outcrops of Palaeozoic rocks in the Axial

Zone have witnessed more than 7000 m of basement stacking (measured between the Balaïtous peak where the top basement crops out and the San Vicente drill core; Fig. 1b; Lanaja 1987). The geometry and kinematics of the thrust units affecting the Palaeozoic rocks are not fully understood because of the complex superposition of deformation events and the unclear relationships with cover units where syntectonic sedimentation plays a key role to assign kinematic ages (Oliva-Urcia 2018). Numerous structural studies (e.g. Muñoz *et al.* 1986, 2019; Muñoz 1992; Puigdefábregas *et al.* 1992; Teixell 1996; Martínez-Peña & Casas-Sainz 2003; Casas *et al.* 2003; Millán *et al.* 2006; Labaume *et al.* 2016; Labaume & Teixell 2018) have identified a general Alpine piggy-back thrust sequence affecting the Palaeozoic rocks (Fig. 2). Besides, numerous fission-track data on granites (Fitzgerald *et al.* 1999; Jolivet *et al.* 2007), on detrital rocks (Beamud *et al.* 2011; Bosch *et al.* 2016; Labaume *et al.* 2016) as well as  $^{40}\text{Ar}/^{39}\text{Ar}$  and U/Pb dating of samples directly taken from fault planes (Abd Elmola *et al.* 2018) and calcite veins (Hoareau *et al.* 2021, see also recent reviews by Oliva-Urcia 2018 and Calvet *et al.* 2020, and references therein), have improved the knowledge on the chronology of emplacement and exhumation of the basement units and their relationship with the cover ones. Basement thrusts partly reactivated previous Variscan, late-Variscan and/or Mesozoic structures. The Alpine structure defines an imbricate thrust system (Fig. 2) with a progressively increasing vertical overlap between the basement units from west (Fig. 2a; Teixell 1996) to east where thrusts define an antiformal stack (Fig. 2c; Muñoz 1992). Basement units in the west include four thrusts in the central sector (Fig. 2b): Millares, Bielsa, Gavarnie and Guarga; and an variable number in the western sector (Fig. 2a), including the Lakora-Eaux Chaudes, Gavarnie, Guara-Gedré, Fiscal-Broto and Guarga thrusts. In the eastern sector (Fig. 2c) three main basement units are recognized, from the north to the south: Nogueras-Gavarnie, Orri and Rialp. In the South Pyrenean Zone, all these basement units connect with an imbricate fold-and-thrust system with different Mesozoic and Cenozoic décollements (Upper/Middle Triassic evaporites, Cretaceous shales and Eocene marls and evaporites); their geometry is controlled by salt-tectonics and Mesozoic inheritance (Huyghe *et al.* 2009; Labaume *et al.* 2016; Oliva-Urcia 2018; Labaume & Teixell 2018; Calvín *et al.* 2018; Santolaria *et al.* 2020).

Thrusting was associated with important foreland flexure and foreland succession deposition both in the Northern Pyrenees (France; Biteau *et al.* 2006) and the Southern Pyrenees (Spain; Puigdefábregas 1975). Foreland deposits partly covered the Palaeozoic units of the Axial Zone in the early orogenic stages and were subsequently exhumed and eroded (Beamud *et al.* 2011; Fillon & Van der Beek 2012). The early, maximum burial conditions in the sampled portion of the Axial Zone are partly constrained by palaeothermal studies in the overlying Meso-Cenozoic cover units (Izquierdo-Llavall *et al.* 2013; Labaume *et al.* 2016). They indicate Cenozoic-age, maximum temperatures of 160–190 °C in the Upper Cretaceous units of the western Axial Zone (Izquierdo-Llavall *et al.* 2013) that increase up to ~250 °C in the Eocene turbidites to the center of the Southern Pyrenean Zone. These values indicate that temperatures in the underlying Palaeozoic rocks could range between 200 and 250 °C during the Cenozoic. Locally, around the Panticosa intrusion, peak burial temperatures may have reached about ~300 °C during the Oligocene (Bosch *et al.* 2016). In the central Axial Zone, thermal models for the Palaeozoic units of the Gavarnie and Orri units reveal peak temperatures below 300°C that were attained during the Early Palaeogene (Waldner 2019). Cenozoic burial favoured the development of Alpine cleavage in the western Axial Zone (Choukroune *et al.* 1973). Conversely, in the

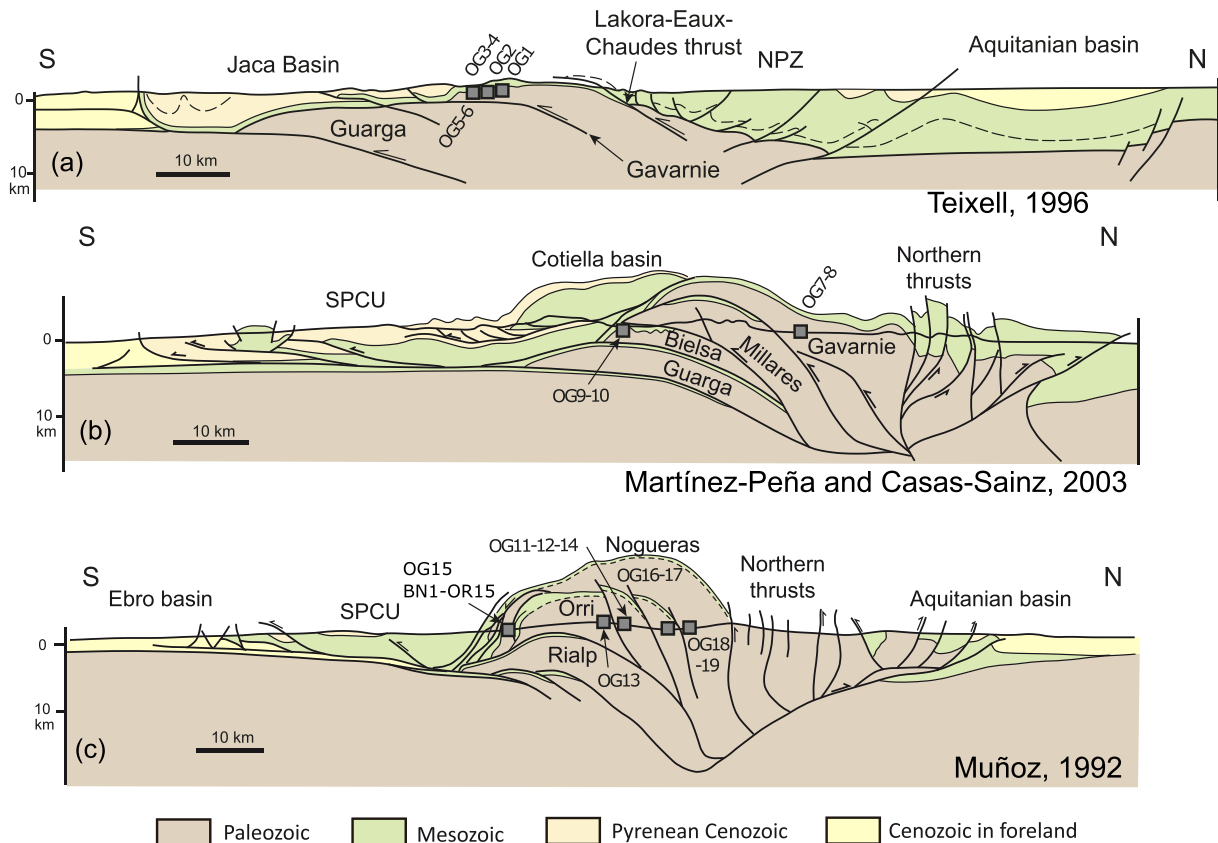


**Figure 2.** Cross sections through the Pyrenees with projected positions of our sampling sites. The cross-section in (a) is from Teixell (1996) whereas cross-sections in (b) and (c) are from Martínez-Peña & Casas-Sainz (2003) and Muñoz (1992), respectively.

central Axial Zone Alpine cleavage developed only locally, the main cleavage being Variscan in age (Muñoz 1992).

### 2.3 Palaeomagnetism in the Pyrenees

Palaeomagnetic investigations in the Pyrenees commenced with the pioneering studies of Van der Lingen (1960) and Schwarz (1963) in some Palaeozoic rocks from the centre of the Pyrenees. The available database has grown substantially during the following decades due to the excellent outcrop conditions (including world class stratigraphic sequences), the general exposure of synorogenic material throughout the chain allowing an accurate dating of deformation, the existence of well-exposed zones of lateral transference of deformation, etc. At present, the Pyrenean chain represents one of the most densely and homogeneously sampled palaeomagnetic databases worldwide (Pueyo *et al.* 2017). Despite the quality and amount of palaeomagnetic data in the Pyrenees, the Pyrenean Palaeozoic rocks have remained largely unexplored. In the Axial Zone, very few data are known from sites older than Permian–Triassic red beds (Van Dongen 1967; McClelland & McCaig 1988, 1989; Keller *et al.* 1994; Tait *et al.* 2000; Gil-Peña *et al.* 2006; Izquierdo-Llavall *et al.* 2014, 2020; Ramón *et al.* 2016). And, to our knowledge, in the Pyrenees only three palaeomagnetic studies collected and analysed a limited number of sites dating from older than late Carboniferous (Stephanian) age: Tait *et al.* (2000), Gil-Peña *et al.* (2006) and Izquierdo-Llavall *et al.* (2020). The two latter studies found the rocks remagnetized in the Late Carboniferous and Palaeogene, respectively. Previous studies in late Carboniferous and

early Permian rocks (Izquierdo-Llavall *et al.* 2014) revealed shallow inclinations and clockwise rotations of ~40°. Gil-Peña *et al.* (2006) showed analogous rotations (~50° CW) for the Ordovician rocks, that probably were remagnetized during late Carboniferous times.

The relatively good palaeomagnetic control on undeformed areas in the vicinity of the Pyrenees (e.g. Garcés *et al.* 2020; Oliva-Urcia & Pueyo 2019) allows to define a reliable reference palaeomagnetic direction and to understand the post-Variscan (late Permian to Eocene) magnetization and tectonic history during the Alpine orogeny in the Pyrenees. In the South Pyrenean Zone, significant rotations both CW and CCW (40–60°) derived from proven primary palaeomagnetic records from rocks of ages ranging from Permo-Triassic (e.g. Larrasoña *et al.* 2003) to Oligocene (e.g. Sussman *et al.* 2004) are found in the most external cover units in relation to lateral ramps in thrust sheets. These rotations are especially evident nearby the boundaries of the so-called South Pyrenean Central Unit (e.g. Sussman *et al.* 2004; Mochales *et al.* 2012, 2016; Muñoz *et al.* 2013; Rodriguez-Pintó *et al.* 2016) but also in the most external thrust units (Pueyo *et al.* 2021a, 2021b). Other moderate vertical axis rotations (15–25° CW and CCW, locally attaining ~40°) occur in the Permo-Mesozoic structural units immediately to the south of the Axial Zone: The Internal Sierras (Larra-Monte Perdido units; Oliva-Urcia and Pueyo 2007a, 2007b; Oliva-Urcia *et al.* 2008; Izquierdo-Llavall *et al.* 2015), the Nogueras thrust and underlying units (McClelland and McCaig 1988, 1989; Dinarès *et al.* 1992; Oliva-Urcia *et al.* 2012; Izquierdo-Llavall *et al.* 2018) and in the eastern Cadi unit (Dinarès *et al.* 1992; Keller *et al.* 1994; Pueyo *et al.* 2016b). In the North Pyrenean Zone (France, Fig. 1b), palaeomagnetic data are scarcer and evidence strong (over 70° CW

in Aptian-Albian rocks, Oliva-Urcia *et al.* 2010; Rouvier *et al.* 2012) to null (Izquierdo-Llavall *et al.* 2020) vertical axis rotations in different areas.

Early Cretaceous remagnetizations are relatively common in the Cretaceous basins deformed to the south of the Axial Zone (e.g. Larrasoña *et al.* 2003; Garcés *et al.* 2016). However, this event has been described, so far, only out of the Axial Zone. These remagnetizations are local and affect compartmentalized and highly subsident basins developed under high thermal gradient conditions (e.g. Lagabrielle *et al.* 2010) which played a key role to chemically remagnetize these rocks (e.g. Dinares-Turell and García-Senz 2000; Gong *et al.* 2008, 2009). On top of that, Cenozoic remagnetizations have been described in the Meso-Cenozoic units just above the Axial Zone (Oliva-Urcia *et al.* 2008, 2012; Izquierdo-Llavall *et al.* 2015). These Cenozoic remagnetizations likely occurred due to the burial associated with the development of the Pyrenean orogenic wedge and southern foreland basin. The wedge generated important lithostatic and tectonic load in the internal units until the final collision, continentalization and exhumation of the Palaeozoic rocks during Oligocene–Miocene times.

Most of the palaeomagnetic data to the south of the Axial Zone recorded, at least partially, Eocene secondary magnetizations (pre, syn and postfolding). Remanent magnetization in the Mesozoic units immediately to the North of the Axial Zone is in general terms post-folding and has been interpreted as a Cenozoic chemical (Oliva-Urcia *et al.* 2010) or thermal (Izquierdo-Llavall *et al.* 2020) remagnetization.

### 3. SAMPLING, METHODS AND RESULTS

We drilled in 19 limestone sites from the Silurian or Devonian, one site of a late Carboniferous-early Permian granite (OG01, Panticosa intrusion) and one Permian dyke that intruded the surroundings of site OG12 (OG12dyke; Fig. 1b; Table 1) with a petrol-powered drill, in total 240 cores. We also collected 6 oriented hand samples (from the OG07 and OG08 sites, three samples each). Sites are distributed along-strike the southern and central Axial Zone from the Gallego valley in the west to the Valira valley in the east in eight different valleys (Fig. 1b; the kml file sample\_locations.kml with exact locations is in the Supplementary material). Sites BN1 and OR15 were collected in the same area of sites published in Tait *et al.* (2000). Several sites allowed field tests: five site-scale fold-tests could be obtained (OG2; OG11; OG13; OG14; OG19); two tilt tests between sites within the same thrust unit (OG3-4; BN1-OR15), and two sites with a baked contact test (OG12 and OG17). We performed all analyses at Palaeomagnetic Laboratory Fort Hoofddijk, Universiteit Utrecht, The Netherlands.

Our sample collection comes from fresh, non-metamorphic and weakly or non-internally deformed sites. Limestones were sedimented in shallow waters usually associated with clastic and pelitic sediments (Casas *et al.* 2019). Most limestone sites contained variable amounts of organic matter visible while drilling. A few of these sites show a spaced solution cleavage and evidence of recrystallization. We collected the bedding orientation and, when observable, that of the pressure-solution cleavage (Table 1).

### 3.1 Alpine tilt estimation

The sampled rocks were affected by both Variscan and Pyrenean orogenies (Alpine). In the Axial Zone, the Pyrenean orogeny produced the development of a south vergent fold-and-thrust system. Its geometry has been extensively investigated in previous studies that reconstruct the Axial Zone structure using a combination of surface data and seismic profiles (Labaume *et al.* 1985; Cámará & Klimowitz 1985; Muñoz 1992; Teixell 1996; Teixell & Muñoz 2000; Matínez-Peña & Casas-Sainz 2003; Izquierdo-Llavall *et al.* 2013; Labaume *et al.* 2016; Muñoz *et al.* 2018; Labaume & Teixell 2018). These studies reveal that the Axial Zone evolves laterally from an imbricate thrust system in the West (Fig. 2a, Teixell 1996) to an antiformal-stack in the East (Fig. 2c, Muñoz 1992). Alpine thrusts are related to kilometric-scale basement folds in their hangingwalls. Basement folding is well recorded by the Mesozoic units unconformably overlying the Palaeozoic rocks and resulted in dominantly southward and northward tilts in the southern and northern part of the Axial Zone, respectively.

We used the available geological maps (GEODE, Robador *et al.* 2019), including numerous bedding data, and published cross-sections to discriminate the effects of Variscan and Pyrenean orogenies and estimate the alpine tilt related to basement thrusting in our sampling sites. In the sites located in the southern part of the Axial Zone, alpine dip directions and dips (Table 1) were estimated from the average orientation of bedding in the Mesozoic units unconformably overlying the Palaeozoic and tested against the dip estimated in cross-sections. Sites in the central part of the Axial Zone (OG11–OG19) are to far away from Mesozoic cover units. In these sites, we defined dip directions as perpendicular to alpine thrusts in the Palaeozoic rocks. Following the dip direction we projected our sampling points into the traces of previously published cross-sections to obtain the dip (Fig. 2). Alpine dips were also estimated considering the Mesozoic geometries reconstructed above the topography in such cross-sections (Fig. 2). Fig. 2 provides a general picture of the structural position of the sampled sites (see corresponding thrust units in Table 1) and the regional alpine tilt recorded by the Mesozoic cover of the Axial Zone. Cross-sections run perpendicular to the main alpine structures and therefore show true alpine dips. Apart from the regional cross-sections shown in Figure 2 (Teixell 1996; Muñoz 1992; Martínez-Peña & Casas-Sainz 2003), we also took into account additional cross-sections located closer to the sampling sites (Izquierdo-Llavall *et al.* 2013, 2018; Labaume & Teixell 2018).

### 3.2 Palaeomagnetic and rock magnetic methods

Knowing when and how rocks magnetized is crucial to obtain an appropriate interpretation of palaeomagnetic results, especially in terms of plate and structural kinematics. In this paper, we combined rock magnetic, palaeomagnetic and structural geology analyses to unravel the magnetization history of the rocks.

Rock magnetism studies the magnetic properties of rocks and their magnetic minerals. The different magnetic properties of rocks, such as magnetic hysteresis, susceptibility and its anisotropy, magnetization versus temperature (thermomagnetic analysis), can inform about the mineral(s) carrying the magnetic remanence and their crystal structure and grain size. This information is the most important to understand the geological processes involved in the magnetization of the rocks, and eventually also a key to unravel magnetization timings. In this research we have performed a series of rock magnetic analyses to fully characterize the magnetic

**Table 1.** Site location and key structural data from each site.

Structure	S0 (Bedding)		Fold axis		S1		Inferred Alpine tilt	Location			
	Dip direction	Dip	Trend	Plunge	Dip direction	Dip		Dip direction	Dip	Latitude	Longitude
OG01	-	-	-	-	-	-	Gavarnie thrust	185	20	42.7473	-0.24 497
OG02*	Fold		191	14	-	-	Gavarnie thrust	185	20	42.7361	-0.25 841
OG03	199	66	287	15	-	-	Gavarnie thrust	185	20	42.7249	-0.28 900
OG04	Fold				20	60	Gavarnie thrust	185	20	42.7259	-0.28 300
OG05*	299	17	-	-	-	-	Gavarnie thrust	180	20	42.7023	-0.12 022
OG06*	358	62	-	-	256	78	Gavarnie thrust	180	20	42.7064	-0.12 464
OG07	36	42	-	-	35	55	Gavarnie thrust	25	45	42.7771	0.19 758
OG08*	10	36	-	-	-	-	Gavarnie thrust	25	45	42.7759	0.19 858
OG09	89	13	-	-	-	-	Bielsa thrust	205	45	42.5673	0.46 444
OG10	17	31	-	-	-	-	Bielsa thrust	205	45	42.5824	0.47 447
OG11	Fold		5	42	-	-	Orri thrust	25	30	42.5222	0.65 244
OG12	40	39	-	-	-	-	Orri thrust	25	30	42.5167	0.65 100
OG13	Fold		32	0	-	-	Orri thrust	25	0	42.5028	0.65 228
OG14*	Fold		292	19	-	-	Orri thrust	25	30	42.4752	0.77 733
OG15	234	48	-	-	-	-	Nogueras thrust units	205	90	42.3380	1.06 883
OG16	16	51	-	-	-	-	Orri thrust	25	45	42.5339	1.17 550
OG17	17	50	-	-	-	-	Orri thrust	25	45	42.5048	1.20 275
OG18	359	51	-	-	254	67	Gavarnie thrust	25	45	42.5689	1.59 106
OG19	Fold		237	5	250	60	Gavarnie thrust	25	45	42.5682	1.58 550
BNI & OR15	185	25	-	-	-	-	Nogueras thrust units	205	90	42.3220	1.10 466

\*Unreliable palaeomagnetic result.

mineralogy of the studied samples as a step towards understanding the magnetization process and timing. We measured 18 high-field thermomagnetic runs in an in-house-built horizontal translation-type Curie balance with a sensitivity of approximately  $5 \times 10^{-9}$  Am $^2$  (Mullender *et al.* 1993) and one in an AGICO KLY-3 susceptibility bridge with a CS2 furnace attachment with nominal sensitivity ( $5 \times 10^{-7}$  SI) and air forced into the tube. This latter analysis included two heating and cooling cycles. We also analysed 20 magnetic hysteresis loops and one first order reversal curve (FORC) diagram. They were measured at room temperature with an alternating gradient force magnetometer (MicroMag Model 2900 with 2 Tesla magnet, Princeton Measurements Corporation, noise level  $2 \times 10^{-9}$  Am $^2$ ). Finally, we obtained 88 isothermal remanent magnetization (IRM) acquisition curves from our Pyrenean limestone samples. Curves were obtained with the robotized magnetometer system of Utrecht University (Mullender *et al.* 2016).

Our palaeomagnetic analyses were focused towards determining the Natural Remanent Magnetization (NRM) of the rocks. NRM provides information about ancient latitudes (inclination of the magnetic remanence) and rotations (declinations with respect to the past north) so that we can constrain the magnetization timing. The NRM of the sample collection was investigated through alternating field (AF) demagnetization and thermal demagnetization. AF demagnetization was carried out using the aforementioned robotic 2G-SQUID magnetometer, through variable field increments (4–10 mT) up to 70–100 mT. In all limestone samples, where high-coercivity, low-blocking temperature minerals (i.e. goethite, titanohematite) were expected, a heating step to 150 °C was performed previous to the AF demagnetization. At the same time this enhances the distinction between secondary and characteristic NRM components determined with AF demagnetization (van Velzen & Zijderveld 1995). In samples demagnetized thermally, a stepwise thermal demagnetization was carried through 10–100 °C increments up to complete demagnetization. Principal component analysis (Kirschvink 1980) was used to calculate magnetic component directions from orthogonal vector endpoint demagnetization diagrams (Zijderveld 1967) with the online open-source software Palaeomagnetism.org (Koymans *et al.* 2016, 2020).

Anisotropy of magnetic susceptibility (AMS) measures the induced magnetization in a rock when applying a magnetic field in

different directions, defining an ellipsoid (e.g. Parés 2015). The shape of the AMS ellipsoid depends on the crystallographic preferred orientation of the minerals; the shape, size and preferred orientation of mineral grains; the occurrence of microfractures, its distribution and size. Frequently it is a good proxy for sedimentary and tectonic fabrics that are not visually obvious, but it is also a powerful method to investigate the effect of deformation on the NRM. We determined the composite fabric of the paramagnetic, diamagnetic and ferromagnetic grains by measuring the AMS of 148 samples from our collection with an AGICO MFK1-FA susceptometer (nominal sensitivity  $2 \times 10^{-8}$  SI).

### 3.3 Rock magnetism results

#### 3.3.1 Thermomagnetic analyses

We placed between 50 and 100 mg of powdered sample material from representative samples into quartz glass cup holders that hold the sample with quartz wool. We programmed stepwise thermomagnetic runs with intermittent cooling between successive heating steps. The heating and cooling segments were 150, 100, 250, 200, 300, 250, 400, 350, 520, 450, 620, 550 and 700 °C and finally back to 25 °C, respectively. Heating and cooling rates were 10 °C min $^{-1}$ . Many samples show a paramagnetic contribution, sometimes uniquely (OG19; Supplementary File SF1), sometimes with a more or less noteworthy alteration reaction at about 400–450 °C. This indicates the presence of non-magnetic sulfides (likely pyrite) that oxidize to magnetite during the thermomagnetic run (Fig. 3; OG14; Supplementary File SF1). Some samples show a small but sharp decay between 500 and 600 °C, indicating the presence of magnetite (Fig. 3, OG13), others show the presence of pyrrhotite with a sudden increase at  $\sim$ 300–320 °C followed by a sharp decrease afterwards (OG8 in Fig. 3; OG06 and OG07 in SF1). All samples showing pyrrhotite contained a less important, but observable, content of pyrite. In the susceptibility versus temperature curve (Fig. 3, BN1), pyrrhotite is observable during cooling but it likely formed as a secondary mineral during one of the heating cycles.

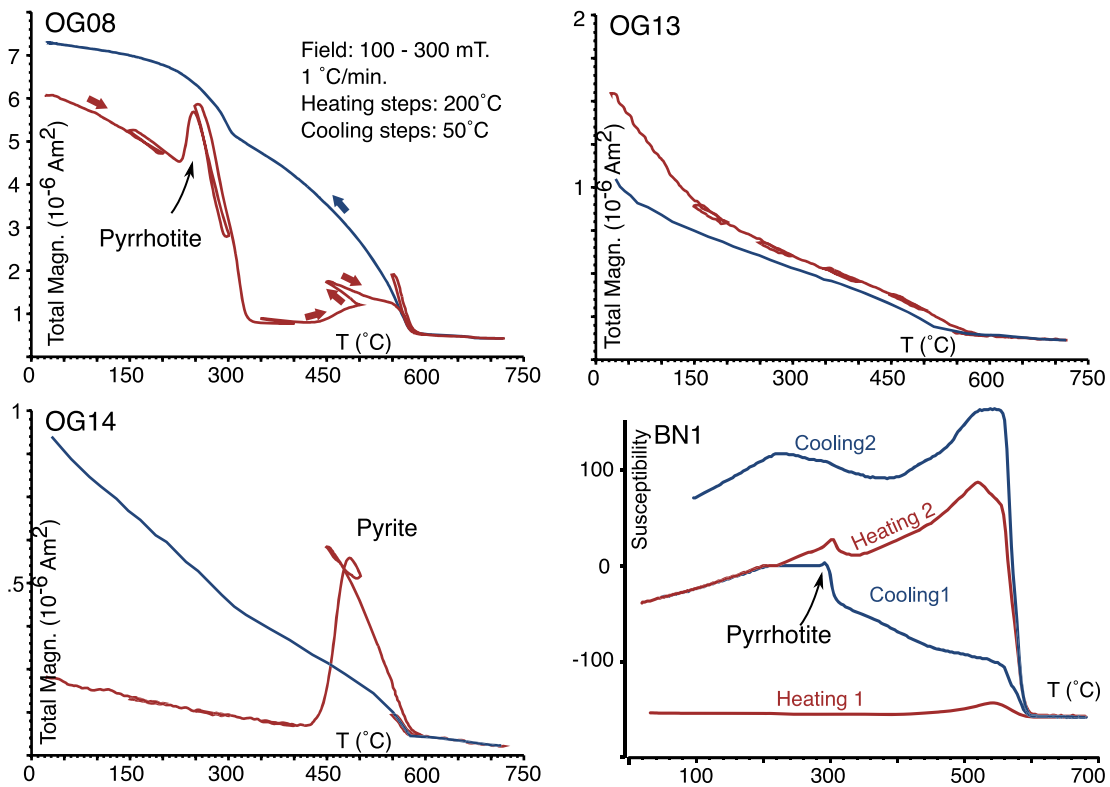


**Figure 3.** Selected magnetization vs. temperature curves (OG8, OG13 and OG14) and susceptibility versus temperature (BN1). Note that magnetic and non magnetic sulfides are common. All measurements performed are available in Supplementary file SF1.

### 3.3.2 Magnetic hysteresis

Representative samples with masses ranging from 20 to 50 mg were measured using a P1 phenolic probe. Hysteresis loops were measured to determine the saturation magnetization ( $M_s$ ), the saturation remanent magnetization ( $M_{rs}$ ) and the coercive force ( $B_c$ ). These parameters were determined after correcting for the paramagnetic contribution. The maximum applied field was 0.5 T. The field increment was 10 mT and the averaging time for each measurement was 0.15 s. We found different loop shapes (Fig. 4, SF-2): (i) Loops that do not saturate at 0.5 T with a pseudo-single-domain like shape which points to the presence of a relatively hard magnetic carrier likely pyrrhotite (Fig. 4, OG08) and (ii) typical magnetite-like pseudo-single domain loops (Fig. 4, OG19). We performed a first order reversal curve (FORC) diagram (Fig. 4, BN1-3) that shows a mixture between superparamagnetic and single domain behaviour.

### 3.3.3 Isothermal remanent magnetization (IRM)

Before the actual IRM acquisition, samples were AF demagnetized with the static 3-axis AF protocol with the final demagnetization axis parallel to the subsequent IRM acquisition field, a procedure that generates IRM acquisition curves with a shape as close to a cumulative-lognormal distribution as possible (Egli 2004; Heslop *et al.* 2004). IRM acquisition curves consist of 61 IRM levels up to 700 mT. The shape of IRM curves is approximately a variably skewed cumulative log-Gaussian function which may contain more than one coercivity phase. IRM component analysis enables a semi-quantitative evaluation of different coercivity components (magnetic minerals or particle sizes) to a measured IRM acquisition curve. Every skewed log-normal curve is characterized by four parameters: (1) The field ( $B_{1/2}$ ) corresponding to the field at

which half of the saturation isothermal remanent magnetization (SIRM) is reached; (2) the magnitude of the phase ( $M_{ri}$ ), which indicates the contribution of the component to the bulk IRM acquisition curve; (3) the dispersion parameter (DP), expressing the width of the coercivity distribution of that mineral phase and corresponding to one standard deviation of the log-normal function (Kruiver *et al.* 2001; Heslop *et al.* 2002) and (4) the skewness of the Gaussian curve (Maxbauer *et al.* 2016). IRM curve unmixing was performed with IRM MaxUnmix package (Maxbauer *et al.* 2016). The interpretation of the coercivity components in terms of mineralogy and grain size is usually done in concert with thermomagnetic curves.

Results from individual samples are characterized by two main IRM components: (i) a relatively soft component (C1 in Fig. 5a) with  $B_{1/2}$  between a minimum value of 23 and a maximum of 74 mT, but generally  $\sim 40$  mT and dispersion parameter (DP) of  $\sim 0.33$  and 0.38 (log units) and (ii) a high coercivity component (C2) with a high  $B_{1/2} > 200$  mT and DP  $\sim 0.5$  (log units). Both components are present in all samples but in varying proportions (Fig. 5A) of the SIRM. We performed end-member modeling in all of the same lithology Silurian-Devonian samples [following the steps of Gong *et al.* (2009a) but without a 150 °C preheating of the samples] to fully characterize the IRM set of samples. The program (Heslop & Dillon 2007) to interpret the IRM acquisition curves uses the algorithm developed by Weltje (1997). End-member modeling assumes that the measured data can be represented by a linear mixture of a number of invariant constituent components, which are referred to as end-members. The algorithm dictates that input IRM acquisition curves are monotonic; the curves were smoothed when appropriate to enforce them being monotonic. By least-squares minimization calculated normative compositions are optimized to the measured

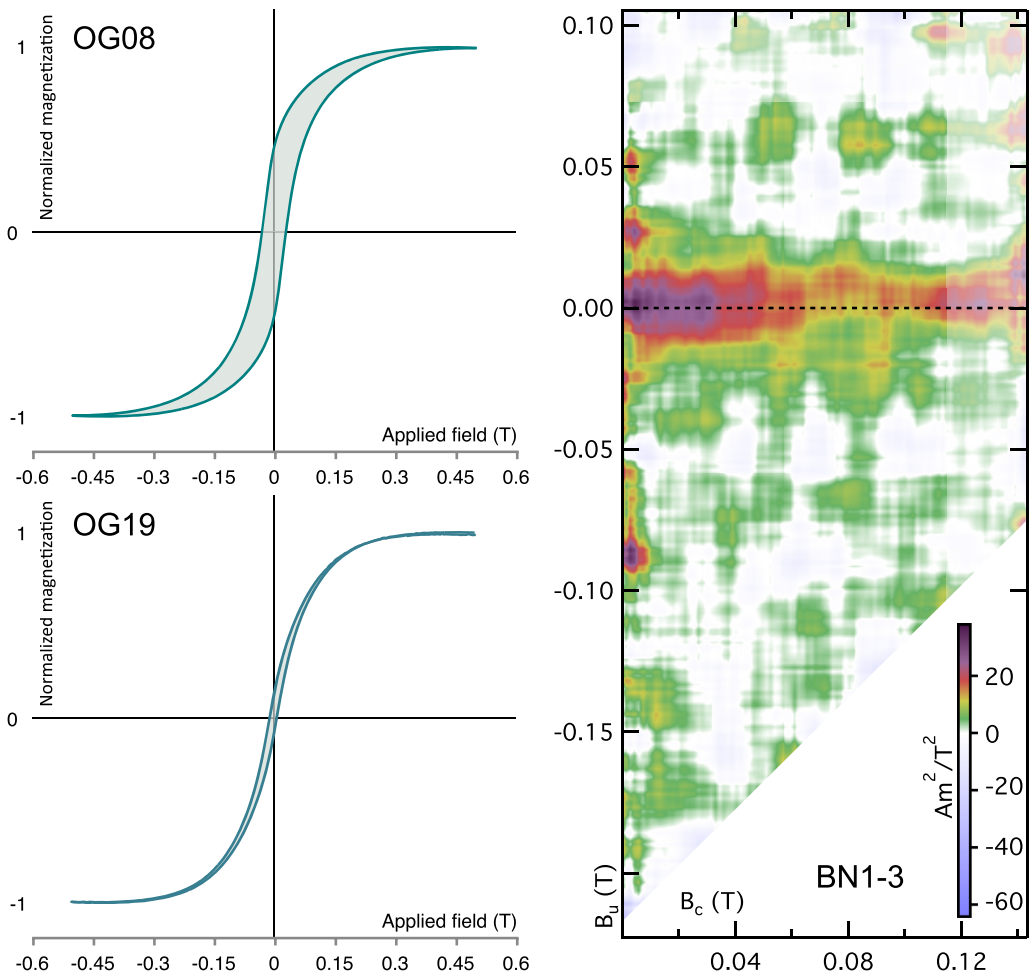


**Figure 4.** Selected slope corrected hysteresis loops and FORC diagram (plotted with FORCINEL (Harrison & Feinberg 2008, smoothing factor 13). All measurements performed are available in Supplementary file SF2.

IRM acquisition curves, eliminating the need for prior knowledge of end-member properties (*cf.* Weltje 1997). For further information about this technique in the framework of remagnetization see the review by Dekkers (2012). We found that a two end-member model shows an acceptable  $r^2$  value of 0.6. Models with 3–9 end-members show slightly better fits ( $r^2 = 0.73\text{--}0.88$ , respectively) although improvement is not deemed that significant (see discussion). The two end-members are a soft (42 mT component with a DP = 0.36) and a hard (a 200 mT component and DP = 0.35) component, analogous to C1 and C2 in the individual IRM curves analysed (Fig. 5c).

### 3.4 Palaeomagnetism results

A minimum of five demagnetization steps was considered to characterize a remanent component. In specimens where directions were difficult to isolate, we used the approach of McFadden & McElhinny (1988) in combining great circles and linear best fits (set points). The virtual palaeomagnetic directions (VPD) software was also used (Ramón *et al.* 2017) at the site level [stacking routine, linearity spectrum analysis, and the virtual direction methods by Scheepers & Zijderveld (1992); Schmidt (1982) and Pueyo (2000), respectively] to confirm the means derived from PCA analyses of individual specimens. Representative Zijderveld diagrams are shown in Fig. 6. For the complete analyses, the reader can check the palaeo-

magnetism.org files associated with this paper (check persistent identifier -PID- in the acknowledgements) and Supplementary File SF3.

Mean directions and uncertainties of each component were evaluated using Fisher's statistics (1953) of virtual geomagnetic poles (VGPs). We applied a fixed 45° cut-off to the VGP distributions of each site. In addition, we used the Deenen *et al.* (2011) criteria to evaluate the scatter of VGPs. As a general rule, if scatter is—mostly—due to palaeosecular variation (PSV) of the geomagnetic field, the associated VGP distribution is roughly circular in shape. However, internal deformation, vertical axis rotation or inclination shallowing may add anisotropy to the scatter. In such cases, VGP distributions will show a certain degree of elongation or are otherwise not spherically uniform. Many samples show a NRM component with very low unblocking temperatures and low coercivities (100–180 °C or 10–12 mT). We consider this component as a viscous remanent magnetization (VRM), because of its similarity to the recent field (Fig. 7 and Supplementary File SF3-a and b).

After VRM removal, the samples show a single NRM component (Fig. 6), generally trending to the origin, regardless of the mineral, magnetite (usually fully demagnetized at 40–60 mT and 500–580 °C) and/or pyrrhotite (fully demagnetized at 330 °C and little to barely demagnetized in AF). This characteristic remanent magnetization (ChRM) clusters well in all the sites (concentration parameter  $k > 8$ , but generally over 15; Table 2; Supplementary

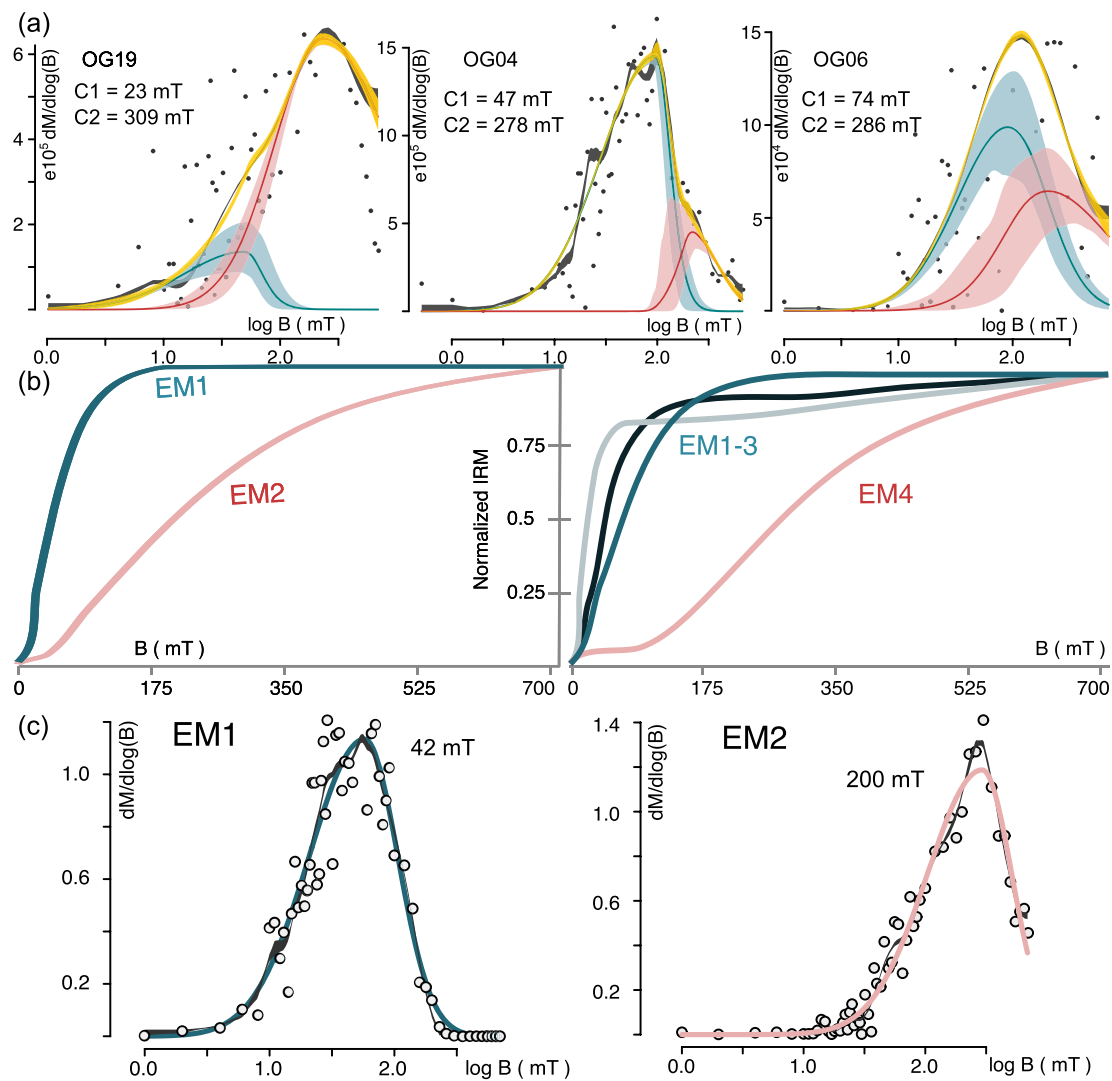


**Figure 5.** (a) Unmixing of IRM acquisition curve for three samples showing different proportions of a ‘soft’ mineral that saturates below 75 mT (magnetite) and a ‘harder’ one that saturates over 200 mT (pyrrhotite). (b) Results from the end-member modeling showing our preferred two end-member solution (left-hand panel) and the four end-member solution (right-hand panel). (c) Unmixing of the IRM synthetic acquisition curve from the two end-members showing the same two magnetic mineralogies as in the forward modeling of different samples: magnetite to the left and pyrrhotite to the right.

file SF3-b) with the exceptions of sites OG02 and OG08 (Figs 8 and 9; Table 2). In addition, there are three sites with less than seven samples passing the 45° cut-off (OG05, OG06 and OG14) and therefore their statistical parameters are not reliable. These five sites were excluded from further interpretation. The remaining 15 sites show quite variable ChRM declinations and inclinations which appear to be only comparable between sites within the same thrust unit (Figs. 2, 8 and 9, Tables 1 and 2). To account for the different events of deformation we have used bedding corrections (Table 2) and fold tests (Fig. 10). In addition, we also performed inclination only statistics (Enkin & Watson 1996; Arason & Levi 2010) to eliminate clustering problems related to vertical axis rotations using both the bedding parameters and our inferred Alpine corrections (see top of Section 3, Tables 1 and 3).

In geographic coordinates sites that passed the quality filter show clusterings that range from  $k$  (concentration parameter)  $\sim 8$  (OG10 and 11) to  $k \sim 188$  (OG19). Site average declinations range from

125° to 297°, the majority of them in the south quadrants with sites OG15 and BN1-OR15 (combined sites separated by 100 m) being the only exceptions (Figs 8 and 9; Table 2). Inclinations range from -50° to 50°. Bedding correction significantly changes the distribution of the site averages, but the scattering in declinations (from 111° to 289°) and inclinations (-65° to 56°) remains (Table 2), which means that magnetization timing is not the same for all samples and/or structural complications are larger than folding.

All fold-tests whose samples passed the aforementioned quality criteria (Fig. 10; OG03-04; OG11; OG13 and OG19) were performed in folds with weakly plunging axes (Table 1; Fig. 11) with the exception of OG11, which in turn is the only one that is not negative (Fig. 10). OG11 shows a better clustering ( $\tau_1$ ) after tilt correction, however, the fold-axis in site OG11 is steeply plunging (the only case; Fig. 10). The performed fold-tests restore deformation as if axes were horizontal. Steeply plunging axis’ folds, therefore usually yield false positives and negative foldtests (e.g. Pueyo

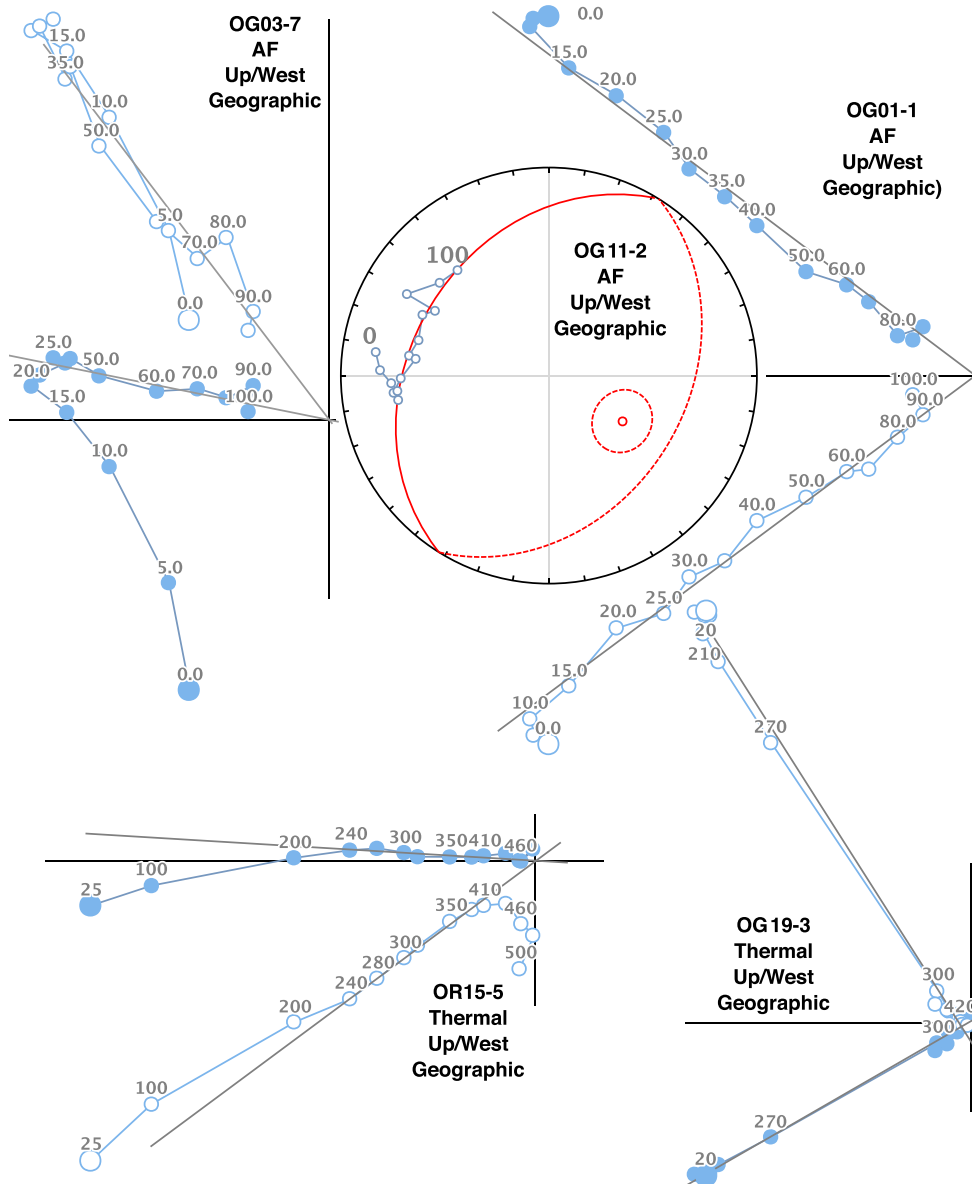


**Figure 6.** Examples of ‘Zijderveld’ vector-end point plots (Zijderveld 1967) for selected samples. All samples plotted in geographic coordinates. Close-open circles represent declination and inclination projections, respectively. Complete analyses are available in palaeomagnetism.org through the Persistent identifier PID given in the acknowledgements.

et al. 2016a). A possibility to decipher the magnetization timing is pre-correcting the plunge of the fold axis before the fold-test. The declination results, in this case, will bring spurious rotations and would not be trustworthy. After back-tilting the plunging-axis in OG11 (azimuth/plunge = 005/42), the fold test remains indeterminate, in this case with a greater clustering ( $\tau_1$ ) before tilt correction [Figs 10 (structural correction panel) and 11]. The statistics of all sites that pass our quality criteria ( $n \geq 7$  and  $k > 8$ ) yield close to random distributions both considering all specimens ( $k = 1.63$  and  $K = 1.65$ ; Supplementary File SF3-A) and the mean of site averages ( $k = 1.95$  and  $K = 2.5$ ; Table 4). As expected from the negative within-site fold-tests, the concentration parameter does not change after bedding correction neither in all specimens together ( $k = 1.51$  and  $K = 1.59$ ; Supplementary

File SF3) nor the mean of site averages ( $k = 1.57$  and  $K = 1.64$ ; Table 4).

Inclination only statistics are independent to differential vertical axis rotations since declinations are not taken into account (e.g. Enkin & Watson 1996). Inclination only statistics were performed on site averages to avoid weighting based on number of specimens (Table 4). The concentration parameter ( $k$ ) equals to 0 in geographic coordinates and 2.17 in tilt corrected coordinates, both figures representing very poor clusterings.  $k$  becomes close to 4 if we do not account for OG3 and OG4, which follow a different trajectory and may represent a different magnetization event (see explanation below). In contrast, when correcting the studied samples exclusively for our inferred Alpine tilt, the inclination only concentration parameter is  $\sim 4$ , but becomes  $\sim 14$  when excluding OG3 and OG4 (Table 4). An inclination only tilt test without OG3 and OG4 shows

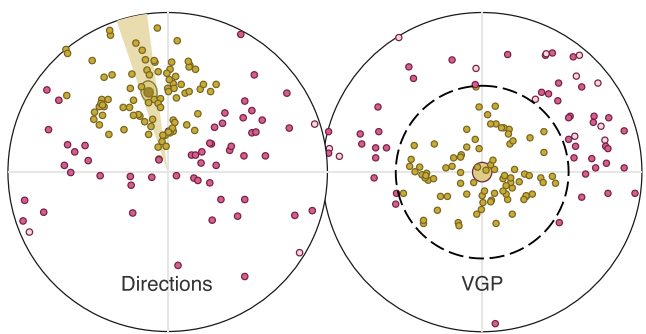


**Figure 7.** Viscous remanent magnetization (VRM) from all samples is compatible with the present-day field (geographic coordinates). Red dots are those that fall outside of the  $45^\circ$  cut-off. Uncertainty envelope is in both cases VGP A95. The rather large scattering is likely due to the small number of demagnetization levels containing the VRM (3–4) and the possible migration of the VRM during transport, storage and analysis.

a best fit for a 110 per cent correction, both using the Enkin & Watson (1996) approach (with a maximum clustering around  $k \sim 12$ ) and a stepwise untilting following Arason & Levi (2010) inclination only statistics with a maximum at  $k \sim 15$  (Fig. 12). OG3 and OG4 share a common true direction in geographic coordinates and their Alpine tilt correction does not change them too much (Fig. 13)

### 3.5 Anisotropy of the magnetic susceptibility (AMS) results

We measured the anisotropy of the magnetic susceptibility in 148 samples from most sites to explore possible causes for the variety of ChRM directions found (Table 2). The degree of anisotropy ( $P$ ) appears to be generally low ( $<1.05$ ; Fig. 14, Supplementary file SF5) although some individual samples showed up to 1.5. The samples' three principal ellipsoid axes (Kmax, Kint and Kmin) mimic the bedding ( $S_0$ , Kmax-Kint fall within the bedding plane and Kmin is perpendicular) in six sites (OG09, 15, 16, 17, 18 and 19); in three samples the AMS ellipsoid corresponded to the foliation  $S_1$  (OG06, 10 and 13); and others showed a quasi-random pattern (OG03, 05, 11, 14) both in geographic and tectonic coordinates (Fig. 14). No observed AMS fabric (not Kmax, Kint or Kmin axes) from the data sets studied coincides with the ChRM directions, suggesting that NRM and ChRM are not significantly biased by rock fabric.

## 4. DISCUSSION

The palaeomagnetic and rock magnetic results obtained from the Silurian–Devonian limestones in the Pyrenees certify that the Palaeozoic rocks from this mountain belt have been subject to at least one widespread remagnetization event. Many samples contain a VRM that is similar to the recent geoaxial dipole for recent times in the Pyrenees (Fig. 7). Apart from this VRM, all rocks, regardless of their magnetic mineralogy, show a single stable component heading to the origin, with the exception of samples not delivering results (Figs 6 and 8). This component is not deviated towards bedding/cleavage planes (as inferred from AMS patterns, Fig. 14) and displays negative fold tests (Fig. 10; perhaps a syn-folding remagnetization in the case of site OG11 where fold test results are indeterminate).

### 4.1 Rock magnetism

Rock magnetic analyses show that both pyrrhotite and magnetite are the magnetic carriers in the Silurian–Devonian limestones whereas magnetite is the carrier in the Panticosa late Carboniferous–Permian granite (OG1) and sampled dyke (OG12dyke). All limestone sites contain variable amounts of pyrrhotite and magnetite as shown both in thermomagnetic curves (Fig. 3), in IRM acquisition curves and during NRM demagnetization (Figs 5 and 6). We applied the IRM end-member modelling technique in an attempt to discriminate between different remagnetization events in the Pyrenees. The two end-member model with a reasonably high  $r^2$  value of 0.65 is our preferred model. Models with 3–9 end-members evidently show slightly better fits ( $r^2 = 0.73$ –0.88, respectively). However, neither the fit improves significantly, nor the shape of the end-members shows more or less anticipated IRM acquisition curves for any particular mineralogy (Fig. 5b). In addition, most of the additional end-members seem to represent the variable coercivity windows of magnetite [e.g. the 4 end-member solution in Fig. 5b: three of the end-members (EM1–3) represent magnetite and do not deliver any particular meaningful result]. All samples contain a significant amount of those additional end-members (varying from 10 to 60 per cent) indicating that a variable grain-size or compositional (Ti-)magnetite is present in virtually every sample. The two end-member model further distinguishes a 42 mT component with a DP = 0.36 (C1), which is typical for magnetite and a 200 mT component and DP = 0.35 (C2), which we interpret as pyrrhotite (Fig. 5c). The two end-members are in agreement with individual sample fits, but end-member IRM acquisition curves describe much better the IRM properties of each magnetic phase (Fig. 5). We interpret the soft component (C1) as magnetite varying from coarse to very fine grained (i.e. lower and higher coercivity, respectively) as supported by hysteresis loops (Figs 4 and SF2). It is reasonable that the high coercivity component (C2) reflects the observed pyrrhotite in the thermomagnetic curves as SD pyrrhotite has a rather high coercivity (Dekkers 1989).

The presence of variable amounts of pyrrhotite and magnetite in all Silurian–Devonian samples studied suggests that this is a common feature for the Palaeozoic sedimentary and metasedimentary units of the mountain belt. Similar to the Pyrenees, pyrrhotite is the most common magnetic carrier in other limestone formations of the Iberian Variscides heavily affected by late Carboniferous magmatism (Pastor-Galán *et al.* 2015a, 2016, 2017; Fernández-Lozano *et al.* 2016).

In general terms, the occurrence of pyrrhotite in limestones is a sign of their remagnetization. Pyrrhotite is a frequent secondary mineral which is formed in low-grade metamorphic rocks under reducing conditions (Crouzet *et al.* 2001; Aubourg *et al.* 2012, 2019; Izquierdo-Llavall *et al.* 2020) or in the presence of non-oxidizing magmatic fluids (Pastor-Galán *et al.* 2016). The occurrence of pyrrhotite has been used as a geothermometer; increasing burial enhances the transformation of magnetite to pyrrhotite and the progressive replacement of magnetite-carried magnetizations by pyrrhotite-carried remagnetizations (e.g. Aubourg *et al.* 2019). In clay-rich rocks, magnetite and pyrrhotite coexist at burial temperatures  $<340$  °C whereas at  $\sim 350$  °C the concentration of magnetite decreases drastically and pyrrhotite becomes the dominant magnetic mineral (Aubourg *et al.* 2019). Izquierdo-Llavall *et al.* (2020) estimated the peak temperatures ( $\sim 350$ – $450$  °C) in the North Pyrenean Zone (between the northermost sides of cross sections 2a and 2b in Fig. 1) following the magnetite–pyrrhotite transformations. In contrast, the temperature estimates for the sampled area, in the

**Table 2.** Palaeomagnetic results for ChRM component for all sites in geographic and tilt (bedding) corrected coordinates.

Geographic	<i>N</i>	<i>Ns</i>	Cut-off	S	Dec	Inc	R	<i>k</i>	a95	K	A95	A95*min	A95max	ΔDx	ΔIx	λ
OG01	10	12	45	16.71	222.7	40.19	9.48	17.27	11.96	24.19	10.02	4.78	19.22	10.89	13.79	22.9
OG02*	6	13	45	30.38	194.24	-4.41	4.97	4.86	33.88	7.34	26.5	5.86	26.52	26.52	52.76	-2.21
OG03	8	8	45	20.23	191.98	-47.6	7.66	20.67	12.47	16.32	14.13	5.22	22.12	16.16	16.7	-28.7
OG04	32	37	45	18.08	184.57	-42.53	30.18	17.02	6.34	20.49	5.75	3	9.24	6.33	7.56	-24.64
OG05*	5	8	45	22.16	5.71	58.01	4.78	17.93	18.57	13.61	21.51	6.3	29.75	28.01	19.81	38.68
OG06*	2	3	45	24.06	248.92	-20.54	1.88	8.48	100.98	11.42	82.51	9.09	52.99	NaN	149.78	-10.61
OG07	11	13	45	21.77	137.77	-32.97	10.37	15.83	11.84	14.29	12.51	4.6	18.1	13.16	19.46	-17.97
OG08*	4	10	45	35.85	263.68	-5.38	3.11	3.36	59.54	5.28	44.25	6.89	34.24	44.31	87.91	-2.7
OG09	13	14	45	21.87	159.34	57.48	12.55	26.68	8.18	14.19	11.4	4.3	16.29	14.55	10.64	38.1
OG10	8	8	45	28.26	179.3	38.56	7.17	8.42	20.28	8.45	20.23	5.22	22.12	21.86	28.68	21.73
OG11	8	8	45	18.26	201.72	-9.18	7.18	8.58	20.06	19.89	12.73	5.22	22.12	12.77	24.98	-4.62
OG12	7	8	45	8.33	125.38	18.71	6.89	53.04	8.36	95.15	6.22	5.51	24.07	6.31	11.48	9.61
OG12-Dyke	4	6	45	16.99	167.95	46.44	3.9	28.77	17.42	23.01	19.57	6.89	34.24	22.23	23.72	27.73
OG13	19	21	45	16.57	255.81	27.7	18.01	18.2	8.09	24.22	6.96	3.7	12.83	7.2	11.67	14.71
OG14*	5	7	45	11.11	27.96	-4.07	4.79	19.12	17.95	53.41	10.56	6.3	29.75	10.57	21.05	-2.04
OG15	15	15	45	6.56	291.06	16.61	14.87	107.25	3.71	152.91	3.1	4.06	14.89	3.14	5.82	8.48
OG16	10	11	45	23.96	197.11	-36.31	9.14	10.48	15.66	11.72	14.72	4.78	19.22	15.71	21.7	-20.18
OG17	10	13	45	12.28	165.55	-41.26	9.79	41.99	7.54	43.86	7.38	4.78	19.22	8.06	9.94	-23.69
OG18	7	11	45	10.29	146.65	-48.47	6.88	49.71	8.64	62.26	7.71	5.51	24.07	8.86	8.94	-29.45
OG19	15	16	45	6.98	151.24	-50.69	14.93	188.02	2.8	135.26	3.3	4.06	14.89	3.87	3.64	-31.41
BN1 & OR15	16	19	45	18.76	297.88	56.61	15.43	26.13	7.35	18.89	8.71	3.96	14.3	10.96	8.32	37.18
Tilt corrected																
OG01	10	12	45	16.71	222.7	40.19	9.48	17.27	11.96	24.19	10.02	4.78	19.22	10.89	13.79	22.9
OG02*	5	13	45	28.84	290.83	0.19	4.02	4.07	43.34	8.09	28.63	6.3	29.75	28.63	57.26	0.1
OG03	8	8	45	24.81	30.57	-65.75	7.66	20.67	12.47	10.9	17.56	5.22	22.12	26.79	13.23	-47.98
OG04	32	37	45	18.27	179.62	-19.66	29.27	11.35	7.89	19.99	5.83	3	9.24	5.92	10.66	-10.13
OG05*	6	8	45	27.91	19.38	45.79	5.54	10.9	21.23	8.67	24.12	5.86	26.52	27.35	29.65	27.2
OG06*	2	3	45	16.59	230.08	-10.25	1.88	8.48	100.98	23.93	53.52	9.09	52.99	53.83	104.49	-5.17
OG07	11	13	45	16.8	156.89	-16.86	10.37	15.83	11.84	23.56	9.61	4.6	18.1	9.72	18	-8.62
OG08*	3	10	45	26.69	247.31	-2.42	2.63	5.46	58.88	9.34	42.85	7.73	41.04	42.86	85.58	-1.21
OG09	13	14	45	17.61	164.17	45.05	12.55	26.68	8.18	21.64	9.12	4.3	16.29	10.21	11.39	26.6
OG10	6	8	45	30.89	169.06	56.53	5.52	10.48	21.7	7.09	27.03	5.86	26.52	34.74	25.85	37.1
OG11	8	8	45	11.72	200.07	-4.48	7.75	27.93	10.66	48.06	8.07	5.22	22.12	8.08	16.07	-2.24
OG12	8	8	45	16.16	111.8	5.44	7.43	12.25	16.48	25.83	11.11	5.22	22.12	11.12	22.06	2.72
OG12-Dyke	4	6	45	19.2	127.4	56.64	3.85	20.52	20.78	18.07	22.22	6.89	34.24	28.35	21.19	37.21
OG13	11	21	45	19.66	183.15	41.74	10.46	18.38	10.94	17.25	11.31	4.6	18.1	12.4	15.1	24.04
OG14*	5	7	45	21.6	46.47	-55.84	4.79	19.12	17.95	14.34	20.91	6.3	29.75	26.32	20.34	-36.39
OG15	15	15	45	5.25	289.1	-11.31	14.87	107.25	3.71	238.05	2.48	4.06	14.89	2.5	4.82	-5.71
OG16	10	11	45	20.18	15.07	-14.68	9.14	10.48	15.66	16.44	12.28	4.78	19.22	12.38	23.37	-7.46
OG17	11	13	45	16.57	171.02	0.43	10.41	16.87	11.45	24.55	9.4	4.6	18.1	9.4	18.8	0.21
OG18	8	11	45	17.99	159.26	-8.83	7.4	11.66	16.93	20.94	12.39	5.22	22.12	12.43	24.35	-4.44
OG19	9	16	45	4.48	155.85	10.2	8.96	217.22	3.5	327.87	2.85	4.98	20.54	2.86	5.56	5.14
BN1 & OR15	14	19	45	21.46	257.17	56	13.43	22.91	8.49	14.47	10.82	4.18	15.55	13.51	10.49	36.55

\*Less than *n* = 7 was not considered.

southern Pyrenees (Izquierdo-Llavall *et al.* 2013; Labaume *et al.* 2016) are much lower (below ~300 °C) and the burial/thermal effect in the formation of pyrothite is expected to be less important. Taking that into account, we suggest that in our samples pyrrhotite could be mainly formed by a fluid induced chemical remagnetization during the latest stages of the Variscan orogeny. However, our westernmost sampled units (OG1–OG4) may have surpassed the Curie temperature of pyrrhotite (~320 °C; e.g. Dekkers 1989) during the Cenozoic burial (Bosch *et al.* 2016), and could, therefore, carry a Cenozoic TRM.

In pyrrhotite, the magnetic easy direction is confined to the basal crystallographic plane which implies an intrinsically strong anisotropy because of the ‘hard’ crystallographic c-axis (Schwarz & Vaughan 1972; Schwarz 1974). When pyrrhotite grows oriented in a preferred fabric (e.g. S1 or S0), the direction of the magnetic remanence can be biased towards the fabric plane (Fuller 1963). The studied samples occasionally show pressure solution cleavage and a widespread presence of pyrrhotite as a partial or main carrier of the NRM. AMS fabrics revealed that pyrrhotite is not oriented according to the S1 fabric, and therefore preclude major biases in the magnetic remanence of such secondary sulfides. Besides, although our

AMS results are frequently consistent with bedding (S0), the magnetic remanence is not contained within bedding planes (Fig. 14; Table 2) which also impedes a deviation of the ChRM towards S0.

## 4.2 Palaeomagnetism and timing of remagnetization

We only considered sites for interpretation with at least 7 specimens passing the VGPs 45° cut-off criterion and with the concentration parameter *k* > 8. Sites OG02, 05, 06, 08, 14 and the dyke in OG12 do not pass these criteria and are not considered for further interpretation (Table 2). The rest of the sites show *k* values that range from barely above 8 in geographic coordinates (OG10 and 11), which could be expected also from detrital magnetizations, to over 40 (OG12, OG15, OG17–OG19) in geographic coordinates, which is unlikely in primary magnetizations of sediments (e.g. Deenen *et al.* 2011). Site averages point generally to ESE–WSW with both positive and negative inclinations in geographic coordinates with the only exceptions of OG15 and BN1-OR15 which point WNW (Figs 8 and 9; Table 2), something that does not change after bedding

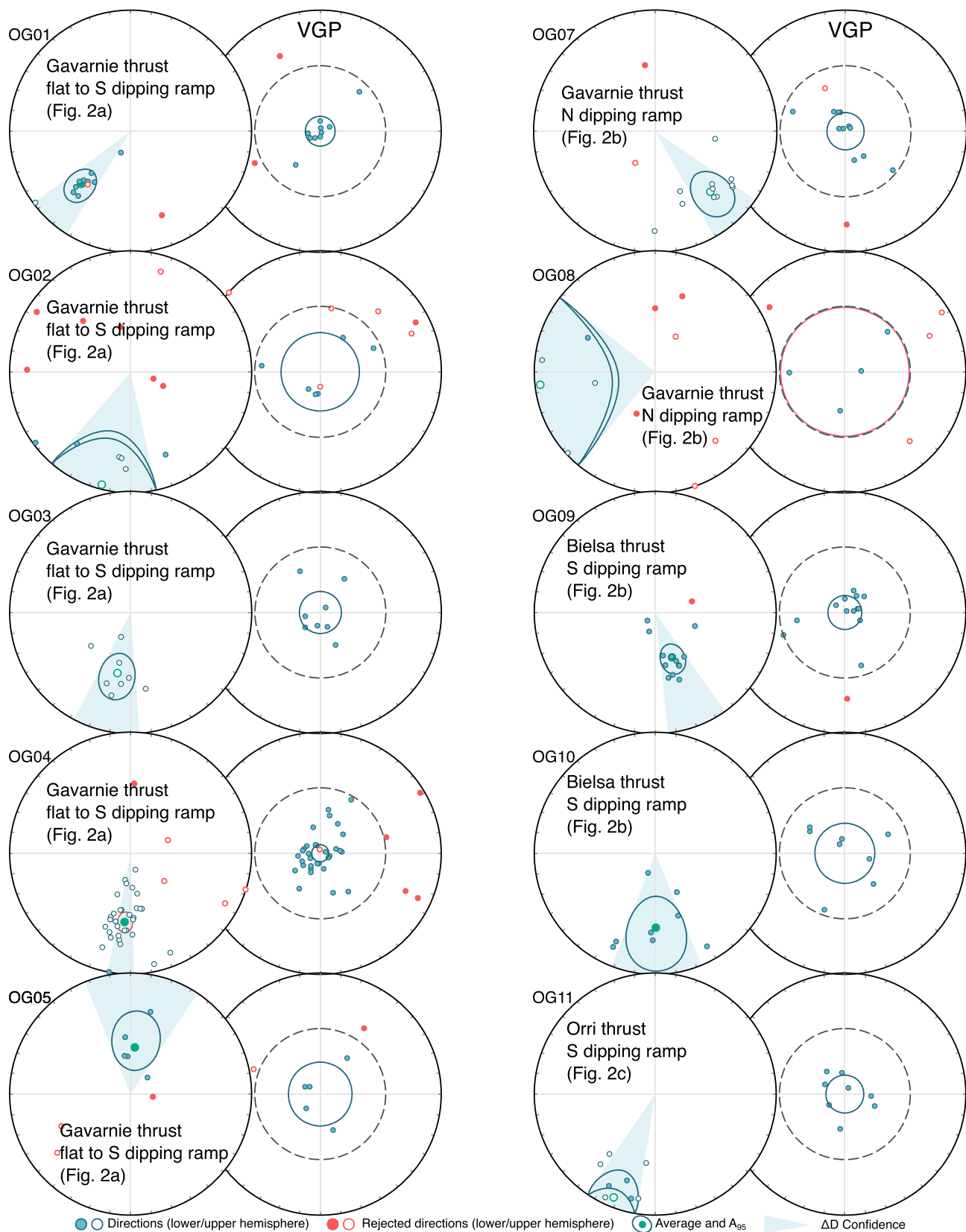


**Figure 8.** Directional and VGP results in geographic coordinates of sites OG01–OG11. Uncertainty envelope is in both cases VGP A95. Red dots are those that fall outside of the  $45^\circ$  cut-off. Sites OG02, 05 and 08 did not provide statistically meaningful results and were not interpreted.

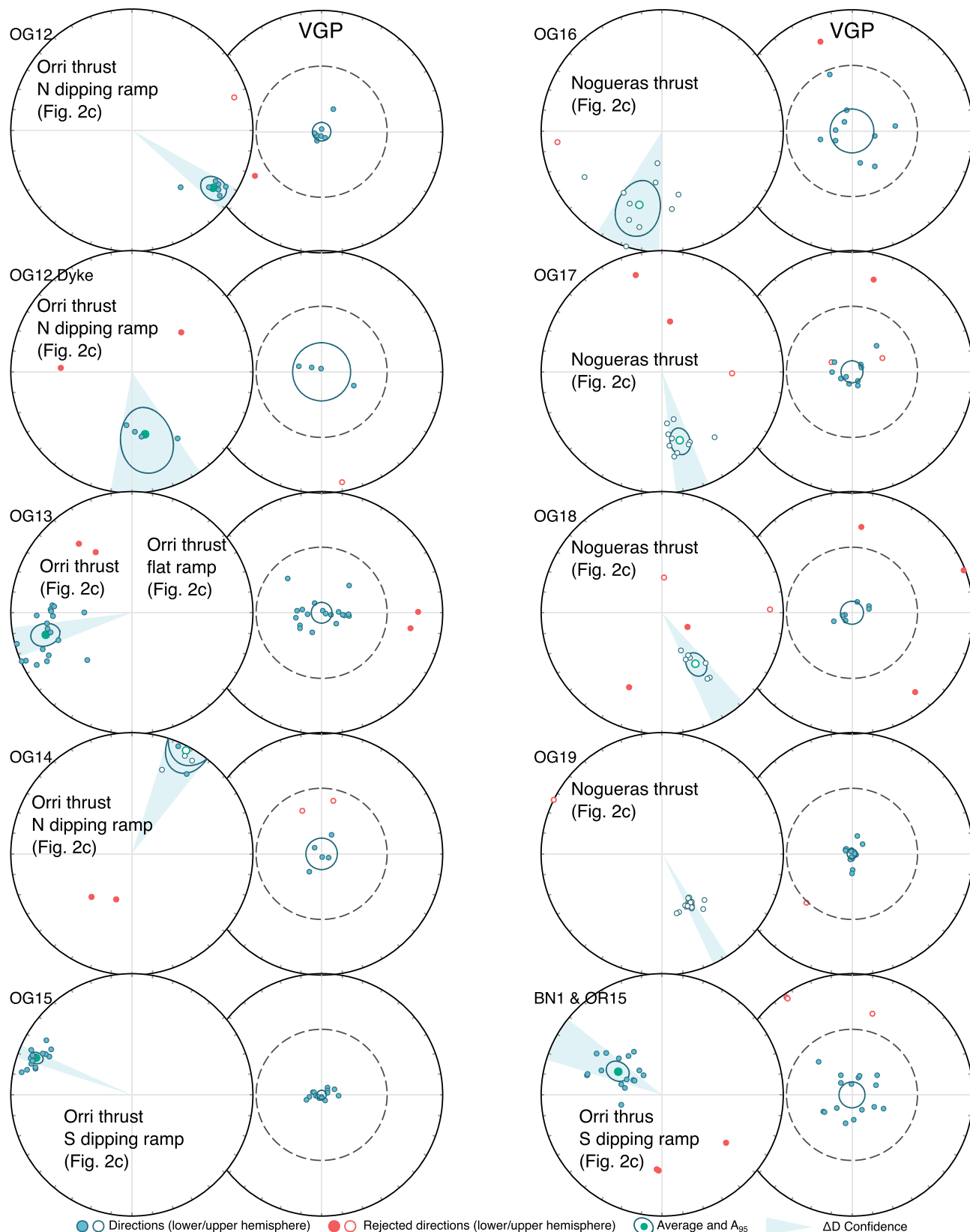


**Figure 9.** Directional and VGP results in geographic coordinates of sites OG12–OG19 and BN1–OR15. Uncertainty envelope is in both cases VGP A95. Red dots are those that fall outside of the 45° cut-off. Sites OG02, 05 and 08 did not provide statistically meaningful results and were not interpreted.

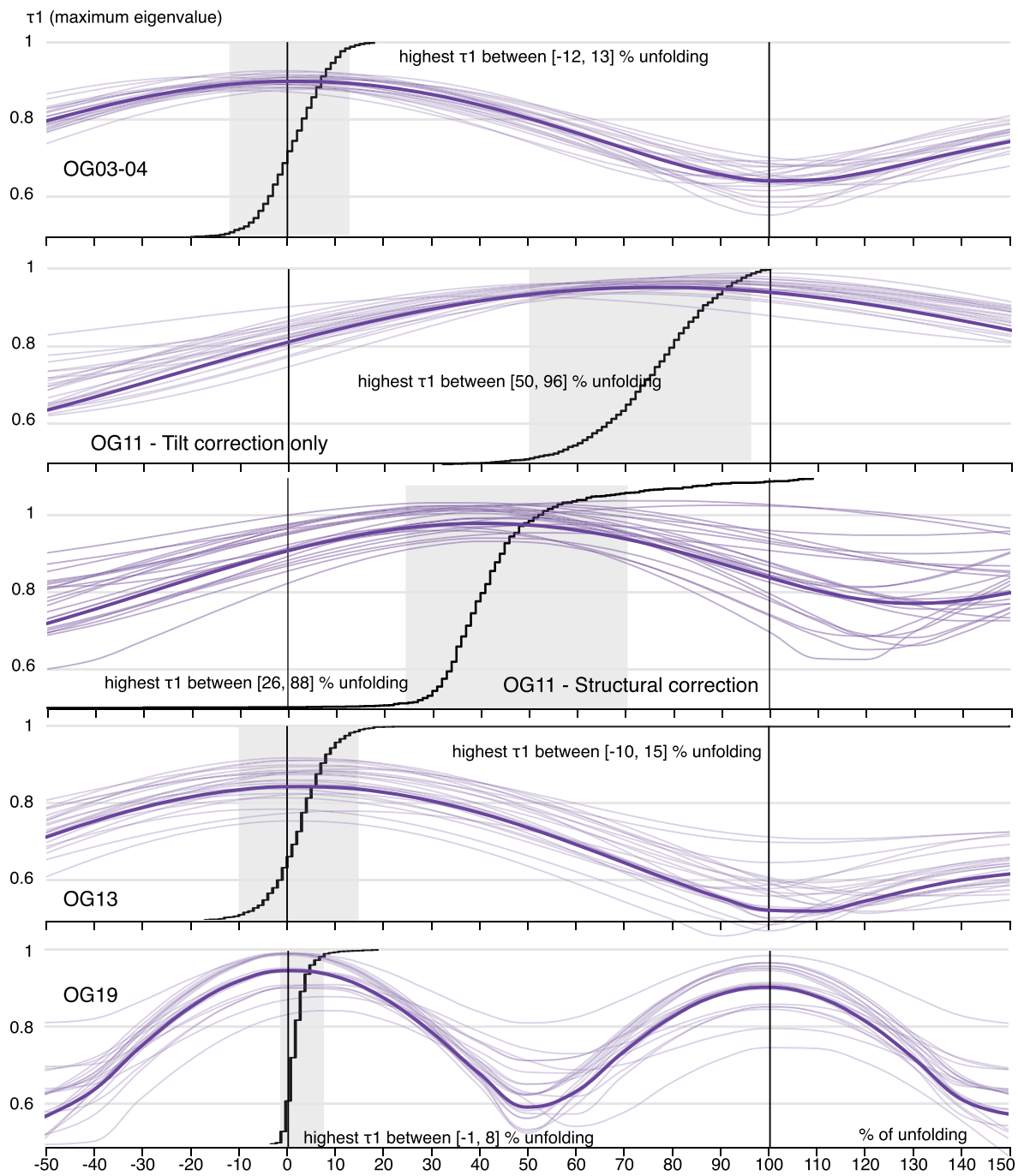


**Figure 10.** Within-site fold tests. All are negative but OG11, which is inconclusive.

correction. With the exception of OG11, we have documented post-folding magnetizations. Importantly, the fabrics do not show consistency with NRM directions (AMS fabric coincident with S1 does not occur and ChRMs are not within bedding planes) suggesting that any potential bias caused by a preferred orientation of pyrrhotite particles is not significant. Therefore, a post Variscan folding (i.e. late Carboniferous) is the oldest possible age for the magnetization since no earlier folding event has been described in the Pyrenees. The OG11 fold, which has a steep plunging axis (Fig. 11), yielded an inconclusive fold-test, but shows better clustering after tilt correction (Fig. 10). Classical fold-tests assume horizontal axes and performing them in steeply plunging axis' folds is unreliable (e.g.

Pueyo *et al.* 2016a). In the case of OG11, pre-correcting the fold axis plunge produces another inconclusive result (Fig. 10). However, declinations in geographic, standard bedding correction, and Alpine tilt correction remain around 200° (Table 2 and 3) and inclinations are in all cases relatively shallow (between  $-9$  and 20°), suggesting that OG11 acquired its NRM during a reversed chron during a time when Iberia was at equatorial latitude: during late Carboniferous or Permian times regardless of the result of the foldtest (e.g. Pastor-Galán *et al.* 2018).

When considering all site palaeomagnetic directions, we found that declinations and inclinations are only compatible in geographic coordinates for those sites within the same tectonic unit

**Table 3.** Palaeomagnetic results (ChRM) after the Alpine tilt correction (tilt associated to the emplacement of the thrusts).

Alpine tilt correction	Dec	Inc
OG01	215.64	23.55
OG03	197.28	-67.34
OG04	184.57	-60.42
OG07	153.46	-8.93
OG09	145.47	21.97
OG10	180.36	-3.3
OG11	185.14	20.77
OG12	110.54	15.53
OG13	255.81	27.7
OG15	278.36	-3.78
OG16	198.58	8.37
OG17	173.76	-6.78
OG18	168.95	-16.46
OG19	172.82	-16.4
BN1 & OR15	238.36	1.58

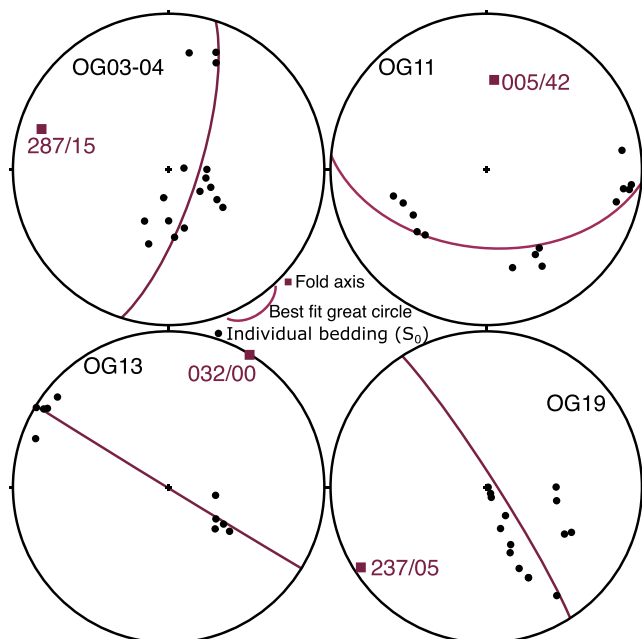


**Figure 11.** Pi diagrams for the studied folds. Only OG11 shows a steeply plunging axis.

**Table 4.** Concentration parameters of inclination only statistics from the mean values of the sites.

Inclination only statistics	<i>k</i>	Inclination	$\alpha_{95}$
Geographic			
Site means avg.	0	0	90
Bedding corrected			
Site means avg.	2.17	18.25	38.91
Site means avg. but OG03 and 04	3.93	22.67	25.44
Alpine tilt corrected			
Site means avg.	4.19	-3.4	21.25
Site means avg. but OG03 and 04	14.42	5.08	11.3

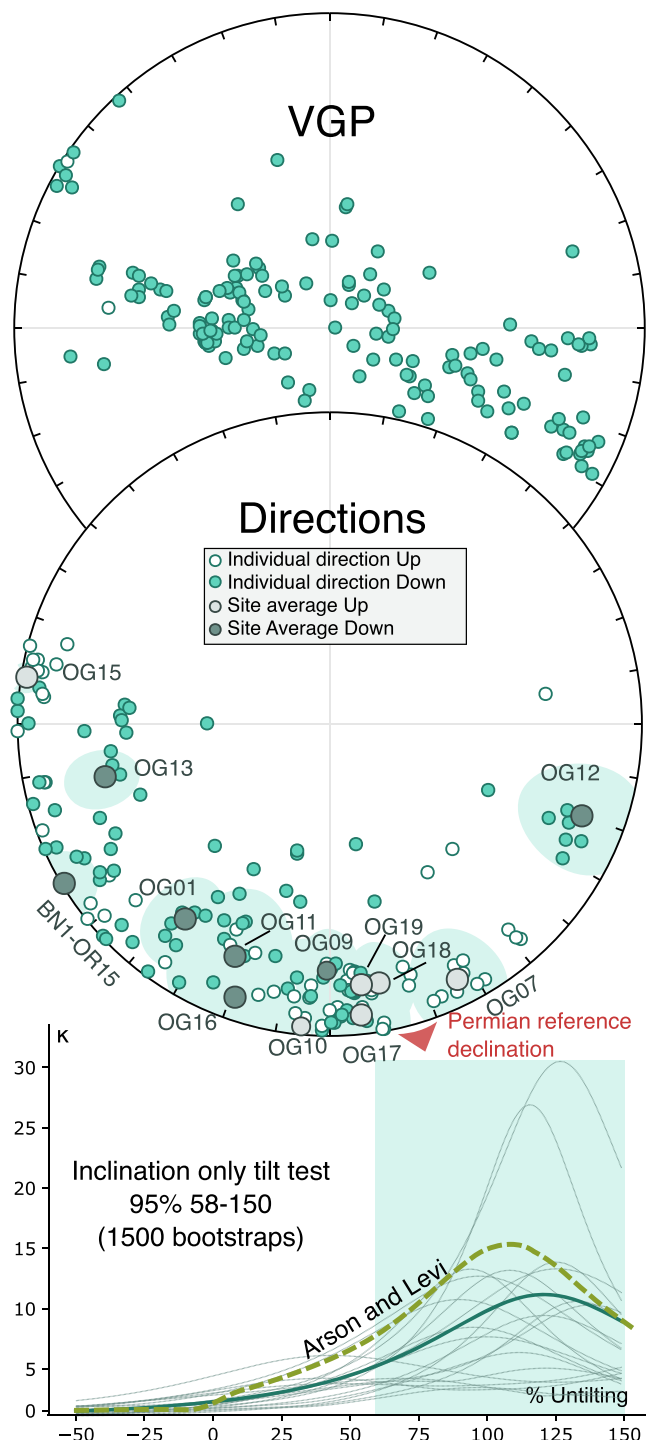


**Figure 12.** Results after the inferred Alpine tilt correction. Permian reference declination for Iberia is after Weil *et al.* (2010). The results show a positive inclination only tilt test following the methodology of Enkin & Watson (1996) (selected bootstraps in thin grey lines) and Arson & Levi (2010) approach (dashed line).

(Figs. 1, 2, 8, 9; Table 2). Such a directional pattern may be indicative of (i) different timing of NRM acquisition for each tectonic unit, (ii) differential vertical axis rotations between units, (iii) post-magnetization differential tilting between units or (iv) a combination of the previous processes. To distinguish between these options inclination only statistics are appropriate (e.g. Enkin & Watson 1996).

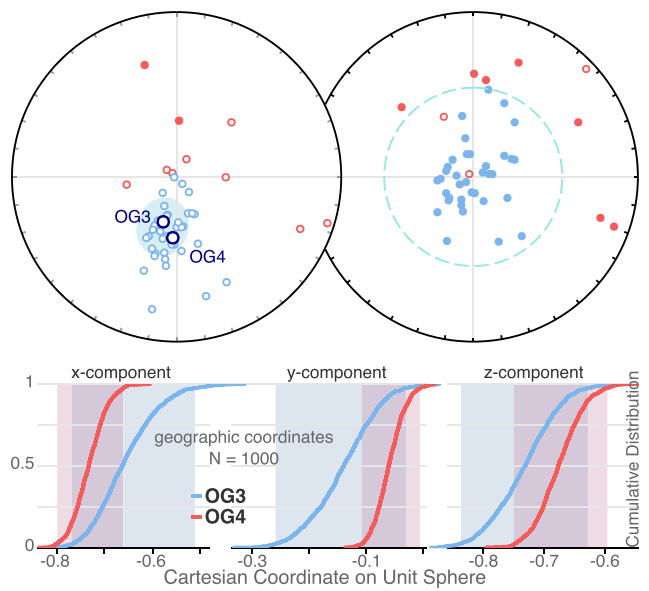


**Figure 13.** OG03 and OG04 show a common true mean bootstrapped direction (after Tauxe 2010) in geographic coordinates (and Alpine tilt corrected, since it is the same for both).

Inclination only statistics do not consider declinations and therefore are independent of variations due to differential vertical axis rotations. In order to evaluate potential timing of magnetization we performed statistical analyses in geographic coordinates, after bedding correction, and also after correction of the tilt related to the emplacement of Alpine basement thrusts (Figs. 2, 12, 13; Tables 3 and 4). The concentration parameter of inclination data ( $k$ ) is 0 in geographic coordinates (Table 4), which could mean that (i) sites magnetized at significantly different geological times when Iberia was at very different latitudes and/or (ii) Alpine tilting postdates the magnetization and therefore it has a strong influence on the inclinations. Inclination only  $k$  is still too low (minimum  $k \sim 8$  to consider an acceptable clustering) after bedding correction ( $\sim 2$ ) but also after Alpine tilt correction ( $\sim 4$ ).

Two sites from the Gavarnie thrust unit (OG03 and OG04; Figs 8 and 13, geographic coordinates) move in a very different direction both during bedding and Alpine tilt corrections. In contrast, OG01 (Panticosa granite, late Carboniferous-Permian, Denèle et al. 2012), which is in the same Gavarnie thrust unit, correlates well with the rest of the sites in all thrust units after Alpine tilt correction but not with the neighbouring OG03 and OG04. Thus, those sites might have acquired their magnetization at a significantly different time than the rest. After removing OG03 and OG04, the inclination only concentration parameter still indicates poor clustering after bedding correction ( $k \sim 4$ ). However, when correcting only for the Alpine tilt  $k$  becomes 14.42 and a positive inclination only tilt test with a maximum in a 110 per cent untilting is obtained (95 per cent between 58 and 150; Fig. 12; Table 4). After the Alpine tilt correction, the mean inclination is  $5^\circ \pm 11$  (Table 4) and all included sites show SW to SE declinations (Fig. 12). Despite the positive result, our Alpine tilt correction should be taken cautiously. We considered only regional tilt values, which were inferred from the average orientation of the overlying Mesozoic units and thrust slopes in geological maps and cross-sections (Fig. 2). Our estimated values took into account the kilometric-scale, thrust-related folding of the basement but can not consider the potential contribution of Alpine, outcrop-scale folding of the Palaeozoic strata.

We believe, however, that the inclination only  $k$  value of 14.42 together with the obtained shallow inclinations and southerly declinations are sufficiently convincing to argue for a common timing of NRM acquisition for the samples included in the tilt test (Fig. 12). The results imply a post-folding but a pre-Alpine tilt NRM. The shallow inclinations suggest that Iberia was located at equatorial latitudes and the southerly declinations suggest that this occurred during a reverse chron. We therefore suggest that all samples that passed the quality criteria, with the exception of sites OG03 and OG04, magnetized during the latest Carboniferous to middle Permian times during the Kiaman reverse superchron, when Iberia was indeed located at equatorial latitudes (Weil et al. 2010). The late Carboniferous and early Permian times in the Pyrenees are characterized by widespread intrusions and volcanism (Panticosa granite, for example, OG01; Gleizes et al. 1998). We hypothesize that the remagnetization mechanism in the Pyrenees was triggered by fluids associated to the magmatic activity analogously to the remagnetizations observed in the Central Iberian Zone of west Iberia (e.g. Fernández-Lozano et al. 2016; Pastor-Galán et al. 2016, 2017).

To further test the hypothesis of a post-Variscan but pre-Alpine orogeny remagnetization with the exception of OG03 and OG04, we have plotted the palaeolatitudes and declinations of OG sites compared to the Global Apparent Polar Wander Path (GAPWaP) of Torsvik et al. (2012) rotated to Iberian coordinates (Pastor-Galán et al. 2018). Palaeolatitudes of OG sites show a good fit and variable clockwise rotations with respect to the declinations expected in Iberia for Carboniferous and early Permian times after Alpine tilt correction, with the exception of OG03 and 04 (Fig. 15a). Whereas, both palaeolatitudes and declinations are scattered in geographic coordinates, in contrast to the expected general good fit if remagnetization had happened after the Alpine orogeny, when Iberia was tectonically stable (Fig. 15b). In geographic coordinates only three sites fit in both palaeolatitude and declinations with the post-Alpine GAPWaP segment: OG3, OG4 and OG16. However, we interpret OG16 as a Permian remagnetization since it fits much better with its neighbouring sites OG17, 18 and 19 after the correction of the alpine tilt.

OG03 and OG04 show a negative fold test (Fig. 10) and a common true mean direction in geographic coordinates (Fig. 13). Their palaeomagnetic direction is, however, significantly different from OG01 that is a late Carboniferous-early Permian site located in the same thrust sheet. OG03 and OG04 show declinations to the south (both in geographic coordinates and after Alpine tilt correction) and upward inclinations of  $-43^\circ$  and  $-48^\circ$  (geographic coordinates) or  $-60^\circ$  and  $-68^\circ$  (after the restoration of the inferred Alpine tilt, respectively). Both geographic and Alpine tilt corrected data indicate a remagnetization when Iberia was located at latitudes between  $25^\circ$  and  $50^\circ$  during a reverse chron (Figs 15a and b). OG03 and 04 results fit best with a remagnetization that postdates the Cretaceous normal superchron (e.g. Izquierdo-Llavall et al. 2015, and references therein, Fig. 15). Inclinations  $>60^\circ$  (i.e. after Alpine tilt corrections) would only be possible when Iberia was located at similar latitudes as at present, fairly long after the Alpine orogeny which ended at Miocene times. In such case, no correction at all should be applied. Therefore, the magnetization has to be syn- to post Alpine tilting to achieve a good palaeolatitudinal fit. Most structural units just above the basement units are remagnetized by tardi-orogenic burial remagnetizations (post-, syn- and pre- Alpine folding) that affected all kinds of rocks (limestones, calcarenites, redbeds, etc., Dinarès et al. 1992; Dinarès 1994; Keller et al. 1994; Oliva-Urcia & Pueyo 2007b; Izquierdo-Llavall et al. 2015, Mujal et al. 2017, etc.) In addition, the burial temperature of OG03 and OG04 could have

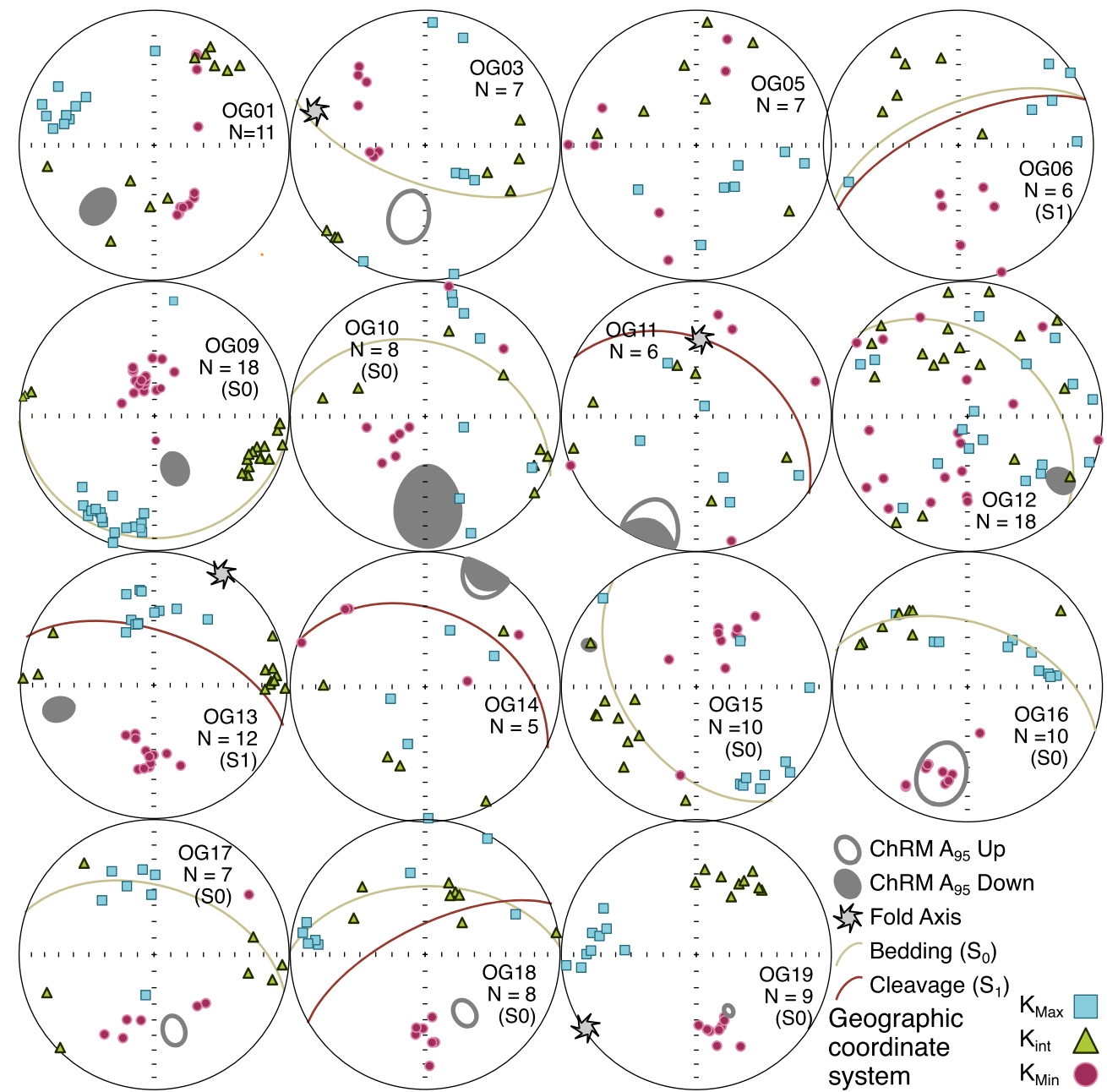


**Figure 14.** Results from the anisotropy of the magnetic susceptibility analyses. Magnetic fabrics represent bedding or S1 cleavage. Magnetic fabric directions do not coincide with the palaeomagnetic directions, which allows us to discard an internal deformation control of the palaeomagnetic remanence.

been sufficiently elevated to trigger a thermal remagnetization after tilting during the unroofing and exhumation of the Axial Zone. With all this elements, we tentatively favour a late orogenic (Eocene) age which would allow inclinations around 50° (close to those obtained in geographic coordinates; Fig. 15b).

#### 4.3 Tectonic significance

The hypothesis of a detachment and northward drift of a peri-Gondwana microcontinent (Armorica s.l.) during the late Silurian or early Devonian (e.g. Torsvik *et al.* 2012; Stampfli *et al.* 2013; Domeier & Torsvik, 2014; Franke *et al.* 2017) is grounded largely on the basis of palaeomagnetic data from the Silurian and Devonian rocks of the Pyrenees (Tait *et al.* 2000), Brittany (Tait *et al.* 1999) and

Bohemian Massif (Tait *et al.* 1994). Our results show that pervasive remagnetizations have affected the Silurian-Devonian limestones of the Pyrenees during, at least, two episodes: late Carboniferous-Early Permian and at the end of the Alpine orogeny. Our site BN1-OR15 was collected in the vicinity of those from Tait *et al.* (2000) and shows the same direction in geographic coordinates (Fig. 9), but within-site clustering worsens after bedding correction (Table 2). After Alpine tilt correction, however, a very good fit results with the majority of our Silurian-Devonian collection. In addition, site BN1-OR15 contains pyrrhotite (Fig. 3), a feature common to all the other samples studied (Fig. 9) and a secondary mineral in (meta)sediments indicative of remagnetization (e.g. Pastor-Galán *et al.* 2017; Izquierdo-Llavall *et al.* 2020). We therefore conclude that the originally published data by Tait *et al.* (2000) also reflect

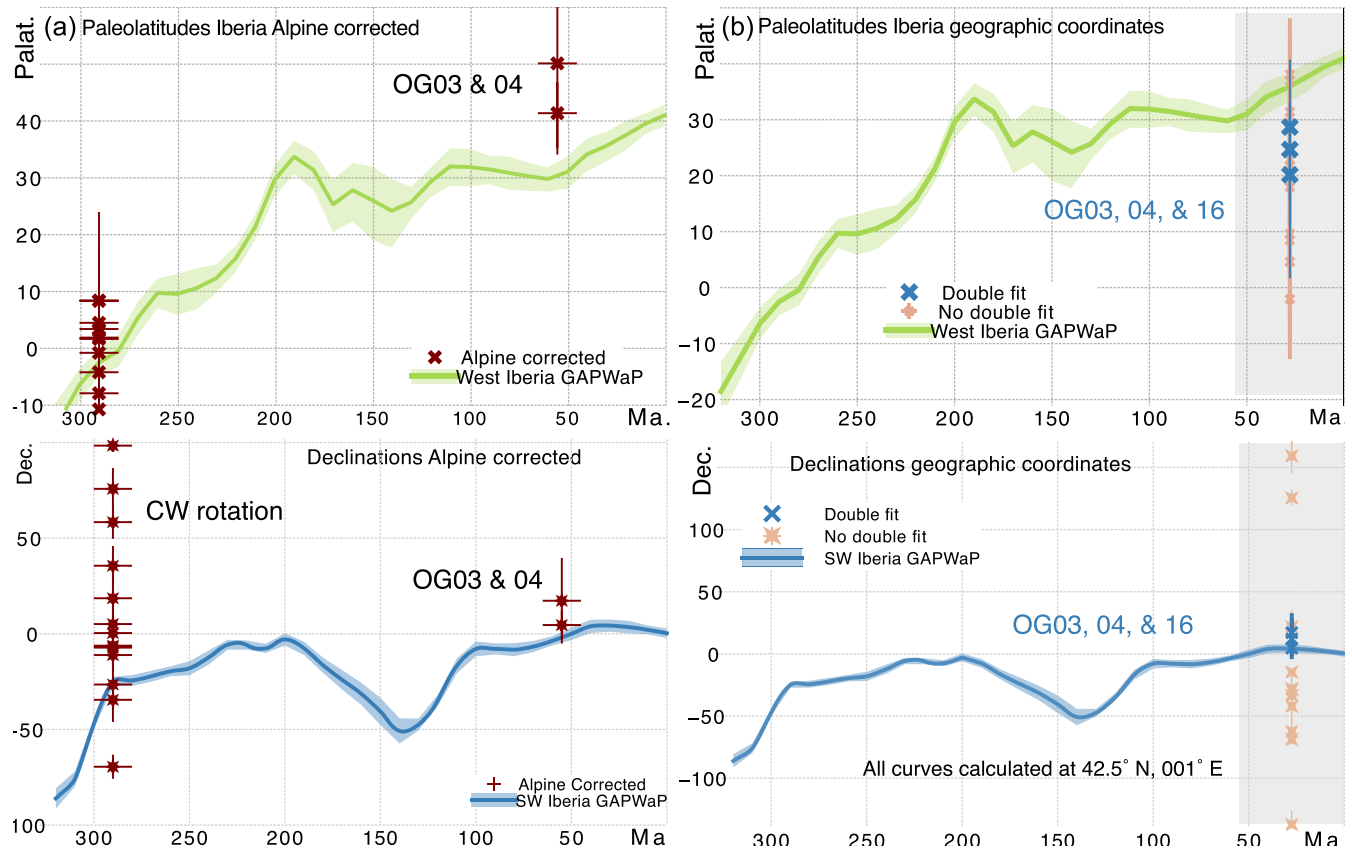


**Figure 15.** Figure showing palaeolatitudes (up) and declinations (down) of OG sites compared to the GAPWaP of Torsvik *et al.* (2012) rotated to Iberia (following Pastor-Galán *et al.* 2018). (a) After Alpine Tilt and (b) Geographic coordinates.

a remagnetization. Since the other palaeomagnetic results from the putative Armorican s.l. continent are similar to those from the Pyrenees and come from areas with intense Carboniferous deformation and enhanced thermal activity, we suspect that they could be remagnetized as well. We request using those palaeolatitudes (Tait *et al.* 1994, 1999) with caution; their palaeomagnetic veracity warrants to be reassessed.

Despite the inherent loss of information due to the remagnetization, especially regarding the potential palaeolatitudinal constraints, the Silurian–Devonian rocks of the Pyrenees do provide interesting insights. Based on the inclination data we interpret that the sampled rocks mostly remagnetized during late Carboniferous and Permian times when Iberia was located around the equator, thus previous to the Alpine orogeny. Our palaeomagnetic results show a positive inclination only fold test when correcting the Alpine tilt inferred from cross-sections and geological maps but negative outcrop scale fold tests when using the bedding parameters. Thus, palaeomagnetism in combination with detailed structural analysis, is a reliable tool to unravel the deformation style of multiphase orogens like the Pyrenees. With our palaeomagnetic data we now can separate the effects of Alpine and Variscan orogeny in the Silurian–Devonian carbonate series, something that classically is deemed challenging (e.g. Casas *et al.* 2019). With our data we can say that the Variscan orogeny was responsible for the main folding event observed in the Silurian and Devonian rocks since all remagnetizations are post-folding (Figs. 10 and 12).

After the Alpine tilt correction, we obtained a relatively good agreement in inclinations, but declinations are still really scattered from SE to SW. Alpine vertical axis rotations in the Pyrenees are

frequent and very variable with magnitudes ranging from a few degrees to up to  $80^\circ$  both clockwise and counterclockwise (e.g. Sussman *et al.* 2004; Rodriguez *et al.* 2016). Although it is plausible that the basement also underwent significant vertical axis rotations, very little is known about the rotational activity of Pyrenean basement thrusts during the Alpine orogeny. The declinations observed in the Silurian–Devonian rocks of the Pyrenees are generally clockwise rotated with respect to the Permian reference pole for stable Iberia (Weil *et al.* 2010; Oliva-Urcia *et al.* 2012). These rotations range from a few degrees to ca.  $90^\circ$  (Fig. 1). We note that such results are also in line with the palaeomagnetic results from Carboniferous and Permian igneous rocks in the Pyrenees and Catalan coastal ranges (Edel *et al.* 2018). The Pyrenees lay in the northern branch of the Cantabrian Orocline, which rotated clockwise during the Late Carboniferous and Early Permian (e.g. Pastor-Galán *et al.* 2015b; Pastor-Galán 2020). Edel *et al.* (2018) interpreted their results as consistent with the rotations expected in the northern branch of the Cantabrian Orocline. Izquierdo-Llavall *et al.* (2014) also found similar data in late Carboniferous and Early Permian rocks of the Pyrenees and interpreted them as an Alpine rotation. We would like to remain wary about their meaning since the variety of rotations found might be reflecting: (i) differential timing of the remagnetization which occurred widely during the Cantabrian Orocline formation as observed in other areas of Iberia (e.g. Pastor-Galán *et al.* 2017, 2020); (ii) vertical axis rotations associated with the Alpine orogeny (Izquierdo-Llavall *et al.* 2014) or (iii) a combination of both processes where the Alpine rotations may be opposite to and/or in the same sense as the late Carboniferous clockwise rotations (Fig. 15).

#### 4.4 A blessing in disguise

The Pyrenees are a multi-orogenic mountain range whose kinematics is often complicated due to the superposition of different deformation events. Accumulation of geological processes, many of them involving relatively high temperatures and fluid percolation increases the chances of remagnetization for the rocks involved in the orogenies. In fact, we suspect that the majority of the Silurian–Devonian carbonate series of the Pyrenees won't preserve any primary and syn-sedimentary magnetization. This makes the Pyrenees, despite the great outcrop quality and quantity, a bad candidate to study pre-Variscan plate motions and kinematics. However, we found generally strong magnetizations containing univocal ChRM, which makes palaeomagnetism of Palaeozoic series in the Pyrenees useful for post-Variscan tectonic studies. Our palaeomagnetic data, in combination with detailed structural observations, has proven an efficient way to unravel the complex tectonic evolution of the Axial Zone of the Pyrenees. We think that at least the Silurian–Devonian carbonate rocks, but likely other Palaeozoic series and igneous rocks are excellent targets to study: (1) the Variscan–Alpine structural relationships, (2) the Alpine rotational history of the basement thrusts and, perhaps (3) the late Variscan deformation events leading to the final amalgamation of Pangea.

### 5. CONCLUSIONS AND CAUTION FOR PALAEOMAGNETISTS

(i) The Silurian–Devonian carbonate series of the Pyrenees show varying amounts of pyrrhotite, a secondary magnetic mineral, and negative fold tests using bedding parameters, which indicate widespread remagnetization(s).

(ii) The majority of sites that passed the quality criteria ( $n > 7$  and  $k > 8$ ) show a positive inclination only fold test when correcting the alpine tilt (with the exceptions of OG03 and OG04). The obtained inclinations are southerly and very shallow, constraining the remagnetization to a reverse chron when Iberia was around the equator, only possible during late Carboniferous or early Permian times.

(iii) Sites OG03 and OG04 (Western Axial Zone, Gavarnie thrust sheet) were likely remagnetized after the main Alpine thrusting, during a pervasive burial remagnetization widely observed in the Internal Sierras and other along-strike equivalent units (Bóixols, Cadí).

(iv) Palaeomagnetism from the Silurian and Devonian rocks suggests that the Variscan orogeny was responsible for their main folding event, whereas the Alpine orogeny produced their thrusting and antiformal stacking.

(v) Our results also show general clockwise rotations which may be consistent with the northern branch of the Cantabrian Orocline. These rotations may as well represent Alpine vertical axis rotations or a combination of both.

(vi) Given the generally good palaeomagnetic quality of the Devonian carbonates, they could be targeted to study the Alpine imprint on Palaeozoic rocks and thus, to unravel the rotational history of basement thrusts.

(vii) The widespread remagnetizations found in the Palaeozoic of the Pyrenees indicate that palaeolatitudes inferred for Silurian and Devonian times from the studied rocks are very unlikely original and should be taken very cautiously. We urge a reassessment of Siluro–Devonian poles from the Variscan in Europe.

(viii) • Palaeomagnetism from multi-orogenic areas is NOT A SIMPLE GAME. However, the systematic combination of palaeomagnetism with detailed structural observations, seems to be a foremost way to unravel complex tectonic evolutions.

### ACKNOWLEDGEMENTS

We really thank the reviewers, Augusto Rapallini and Roberto Molina-Garza for their thorough, positive and very constructive reviews, which in turn made of our work a much better one. This work was funded by postdoctoral (ISES) grant from NWO to DPG and the projects DR3AM, MAGIBER II and UKRIA4D (CGL2014-54118-C2-2, CGL2017-90632-REDT and PID2019-104693GB-I00/CTA) from the Spanish Ministry of Science and Technology. We thank Mat Domeier for providing help with the inclination only statistics. DPG thanks Edward Lodewijk Van Halen for helping all times, we will keep on jumping.

### DATA AVAILABILITY STATEMENT

All data is included in the paper and supplementary materials. In Addition, palaeomagnetic data is stored in palaeomagnetism.org under the persistent identifier (PID) 1871091757a6ef9d46ac59bb9f35c7a6387bc8fcece7bf0715eaba29164fb7e and can be accessed in the link <https://www.paleomagnetism.org/library/>.

### REFERENCES

- Abd Elmola, A., Buatier, M., Monié, P., Labaume, P., Trap, P. & Charpentier, D. 2018. 40Ar/39Ar muscovite dating of thrust activity: a case study from the Axial Zone of the Pyrenees. *Tectonophysics*, **745**, 412–429.
- Arason, J. & Levi, S. 2010. Maximum likelihood solution for inclination-only data in paleomagnetism. *Geophys. J. Int.*, **182**, 753–771.
- Aubourg, C., Jackson, M., Ducoux, M. & Mansour, M. 2019. Magnetite-out and pyrrhotite-in temperatures in shales and slates. *Terra Nova*, **31**(6), 534–539.
- Aubourg, C., Pozzi, J.-P. & Kars, M. 2012. Burial, claystones remagnetization and some consequences for magnetostratigraphy. *Geol. Soc., Lond., Spec. Publ.*, **371**, 181–188.
- Autran, A. & García-Sansegundo, J. 1996. Tectonique hercynienne. Carte structurale (moitié occidentale), in *Synthèse géologique et géophysique des Pyrénées*, Vol. 1, eds Barnolas, A. & Chiron, JC, BRGM-ITGE.
- Azor, A., Dias da Silva, I., Gómez Barreiro, J., González-Clavijo, E., Martínez Catalán, J.R., Simancas, J.F., Martínez Poyatos, D. et al. 2019. Deformation and structure. in *The Geology of Iberia: A Geodynamic Approach*, Regional Geology Reviews, pp. 307–348, eds Quesada, C. & Oliveira, J.T., Springer International Publishing, doi:10.1007/978-3-030-10519-8\_10.
- Barnolas, A. et al., 2019. Alpine foreland basins. In *The geology of Iberia: A geodynamic approach*, Springer, Cham., 7–59.
- Barnolas, A., Gil-Peña, I., Alfageme, S., Ternet, Y., Baudin, T. & Lamonier, B. 2008. Mapa geológico de los Pirineos a escala 1:400 000. IGME/BRGM ISBN: 978-2-7159-2168-9.
- Beamud, E., Muñoz, J. A., Fitzgerald, P. G., Baldwin, S. L., Garcés, M., Cabrera, L. & Metcalf, J. R. 2011. Magnetostratigraphy and detrital apatite fission track thermochronology in syntectonic conglomerates: constraints on the exhumation of the South-Central Pyrenees. *Basin Res.*, **23**(3), 309–331.
- Biggin, A.J., Piispa, E.J., Pesonen, L.J., Holme, R., Paterson, G.A., Veikkolainen, T. & Tauxe, L. 2015. Palaeomagnetic field intensity variations suggest Mesoproterozoic inner-core nucleation. *Nature*, **526**, 245–248.
- Biteau, J.J., Le Marrec, A., Le Vot, M. & Masset, J.M., 2006. The aquitaine basin, *Petroleum Geoscience*, **12**(3), 247–273.

- Bosch, G. V., Teixell, A., Jolivet, M., Labaume, P., Stockli, D., Domènec, M. & Monié, P. 2016. Timing of Eocene–Miocene thrust activity in the Western Axial Zone and Chainons Béarnais (west-central Pyrenees) revealed by multi-method thermochronology. *C.R. Geosci.*, **348**(3–4), 246–256.
- Calvet, M., Gunnell, Y. & Laumonier, B. 2020. Denudation history and palaeogeography of the Pyrenees and their peripheral basins: an 84-million-year geomorphological perspective. *Earth Sci. Rev.*, **103**436.
- Calvín, P., Santolaria, P., Casas, A. M. & Pueyo, E. L. 2018. Detachment fold vs. ramp anticline: a gravity survey in the southern Pyrenean front (External Sierras). *Geol. J.*, **53**(1), 178–190.
- Cámara, P. & Klimowitz, J. 1985. Interpretación geodinámica de la vertiente centro-occidental surpirenaica (Cuenca de Jaca-Tremp). *Estudios geológicos*, **41**(5–6), 391–404.
- Casas, A. M., Oliva, B., Román-Berdiel, T. & Pueyo, E. 2003. Basement deformation: tertiary folding and fracturing of the Variscan Bielsa granite (Axial zone, central Pyrenees). *Geodinamica Acta*, **16**(2–6), 99–117.
- Casas, J.M., Álvaro, J.J., Clausen, S., Padell, M., Puddu, C., Sanz-López, J., Sánchez-García, T. et al. 2019. Palaeozoic basement of the Pyrenees. In *The Geology of Iberia: A Geodynamic Approach*, Regional Geology Reviews, pp. 229–259, eds Quesada, C. & Oliveira, J.T., Springer International Publishing, doi:10.1007/978-3-030-10519-8\_8.
- Choukroune, P. & Séguet, M. 1973. Carte structurale des Pyrénées, 1/500.000, Université de Montpellier – ELF Aquitaine.
- Choukroune, P., Seguret, M. & Galdeano, A., 1973. Caractéristiques et évolution structurale des Pyrénées; un modèle de relations entre zone orogénique et mouvement des plaques, **7**, 600–611.
- Crouzet, C., Stang, H., Appel, E., Schill, E. & Gautam, P. 2001. Detailed analysis of successive pTRMs carried by pyrrhotite in Himalayan metacarbonates: an example from Hidden Valley, Central Nepal. *Geophys. J. Int.*, **146**(3), 607–618.
- Debon &, Guitard. 1996. Métamorphisme et plutonisme hercyniens. Carte de synthèse, in *Synthèse géologique et géophysique des Pyrénées*, Vol. 1, eds Barnolas, A & Chiron, JC, BRGM-ITGE.
- Deenen, M.H.L., Langereis, C.G., Hinsbergen, D.J.J. van & Biggin, A.J. 2011. Geomagnetic secular variation and the statistics of palaeomagnetic directions. *Geophys. J. Int.*, **186**, 509–520.
- Dekkers, M. J. 1989. Magnetic properties of natural pyrrhotite. II. High- and low-temperature behaviour of Jrs and TRM as function of grain size. *Phys. Earth planet. Inter.*, **57**, 266–283.
- Dekkers, Mark J. 2012. End-member modelling as an aid to diagnose remagnetization: a brief review. *Geol. Soc., Lond., Spec. Publ.*, **371**, 253–269.
- Denèle, Y., Paquette, J.L., Ph, Olivier & Barbey, P. 2011. Permian granites in the Pyrenees: the Aya pluton (Basque Country). *Terra Nova*, 1–9.
- Denèle, Y., Laumonier, B., Paquette, J. L., Olivier, P., Gleizes, G. & Barbey, P. 2014. Timing of granite emplacement, crustal flow and gneiss dome formation in the Variscan segment of the Pyrenees. *Geol. Soc., Lond., Spec. Publ.*, **405**(1), 265–287.
- Denèle, Y., Paquette, J.L., Olivier, P. & Barbey, P., 2012. Permian granites in the Pyrenees: the Aya pluton, *Terra Nova*, **24**(1), 105–113.
- Dias da Silva, Í., González Clavijo, E. & Díez-Montes, A. 2020. The collapse of the Variscan belt: a Variscan lateral extrusion thin-skinned structure in NW Iberia. *Int. Geol. Rev.*, **00**, 1–37, Taylor & Francis. doi:10.1080/00206814.2020.1719544.
- Dinarès, J., McClelland, E. & Santanach, P. 1992. Contrasting rotations within thrust sheets and kinematics of thrust tectonics as derived from palaeomagnetic data: an example from the Southern Pyrenees, in *Thrust Tectonics*, pp. 265–275, Springer.
- Dinares-Turell, J. 1994. Remagnetizaciones asociadas y su relación con el emplazamiento de láminas cabalgantes en el Pirineo Meridional, *Geogaceta*, **15**, 105–108.
- Dinares-Turell, J. & García-Senz, J. 2000. Remagnetization of Lower Cretaceous limestones from the southern Pyrenees and relation to the Iberian Plate geodynamic evolution. *J. geophys. Res.*, **105**(B8), 19–19,418.
- Domeier, M. 2016. A plate tectonic scenario for the Iapetus and Rheic Oceans. *Gondwana Res.*, **36**, 275–295.
- Domeier, M. & Torsvik, T.H. 2014. Plate tectonics in the late Paleozoic. *Geosci. Front.*, **5**, 303–350.
- Domeier, M. & Torsvik, T.H. 2019. Full-plate modelling in pre-Jurassic time. *Geol. Mag.*, **156**, 261–280.
- Edel, J.B., Schulmann, K., Lexa, O. & Lardeaux, J.M. 2018. Late Palaeozoic palaeomagnetic and tectonic constraints for amalgamation of Pangea supercontinent in the European Variscan belt. *Earth Sci. Rev.*, **177**, 589–612.
- Egli, R. 2004. Characterization of individual rock magnetic components by analysis of remanence curves. *Phys. Chem. Earth*, **29**, 851–867.
- Enkin, R. J. & Watson, G. S. 1996. Statistical analysis of palaeomagnetic inclination data. *Geophys. J. Int.*, **126**(2), 495–504.
- Fernández-Lozano, J., Pastor-Galán, D., Gutiérrez-Alonso, G. & Franco, P. 2016. New kinematic constraints on the Cantabrian orocline: a paleomagnetic study from the Peñalba and Truchas synclines, NW Spain. *Tectonophysics*, **681**, 195–208.
- Fernández-Suárez, J., Gutiérrez-Alonso, G., Pastor-Galán, D., Hofmann, M., Murphy, J.B. & Linnemann, U. 2014. The Ediacaran-Early Cambrian detrital zircon record of NW Iberia: possible sources and paleogeographic constraints. *Int. J. Earth Sci.*, **103**, 1335–1357.
- Fillon, C. & van der Beek, P. 2012. Post-orogenic evolution of the southern Pyrenees: constraints from inverse thermo-kinematic modelling of low-temperature thermochronology data. *Basin Res.*, **24**(4), 418–436.
- Fisher, R. 1953. Dispersion on a sphere. *Proc. R. Soc., A*, **217**, 295–305.
- Fitzgerald, P.G., Muñoz, J. A., Coney, P. J. & Baldwin, S. L. 1999. Asymmetric exhumation across the Pyrenean orogen: implications for the tectonic evolution of a collisional orogen. *Earth planet. Sci. Lett.*, **173**(3), 157–170.
- Franke, W., Cocks, L.R.M. & Torsvik, T.H. 2017. The Palaeozoic Variscan oceans revisited. *Gondwana Res.*, **48**, 257–284.
- Fuller, M. D. 1963. Magnetic anisotropy and paleomagnetism. *J. geophys. Res.*, **68**(1), 293–309.
- Garcés, M., García-Senz, J., Muñoz, J.A., López-Mir, B. & Beamud, E., 2016. Timing of magnetization and vertical-axis rotations of the Cotilla massif, *Geological Society, London, Special Publications*, **425**(1), 213–232.
- Garcés, M., López-Blanco, M., Valero, L., Beamud, E., Muñoz, J. A., Oliva-Urcia, B. & Cabrera, L. 2020. Paleogeographic and sedimentary evolution of the South Pyrenean foreland basin. *Mar. Pet. Geol.*, **113**, 104105.
- García-Sansegundo, J., Poblet, J., Alonso, J.L. & Clariana, P. 2011. Hinterland-foreland zonation of the Variscan orogen in the Central Pyrenees: comparison with the northern part of the Iberian Variscan Massif. *Geol. Soc., Lond., Spec. Publ.*, **349**, 169–184.
- Gil-Peña, I., Oliva, B., Pueyo, E. L. & Barnolas, A. 2006. Remagnetización Stefanense-Pérmita del Ordovícico de la Zona Axial meridional del Pirineo Central; implicaciones paleogeográficas y tectónicas posthercínicas, in *Proceedings MAGIBER IV- IV Paleomagnetismo en España y Portugal (Vigo)*, pp. 47–50.
- Gleizes, G., Crevon, G., Asrat, A. & Barbey, P., 2006. Structure, age and mode of emplacement of the Hercynian Bordères-Louron pluton, *International Journal of Earth Sciences*, **95**(6), 1039–1052.
- Gleizes, G., Leblanc, D. & Bouchez, J. L. 1997. Variscan granites of the Pyrenees revisited: their role as syntectonic markers of the orogen. *Terra Nova*, **9**(1), 38–41.
- Gleizes, G., Leblanc, D., Santana, V., Olivier, P. & Bouchez, J. L. 1998. Sigmoidal structures featuring dextral shear during emplacement of the Hercynian granite complex of Cauterets–Panticosa (Pyrenees). *J. Struct. Geol.*, **20**(9–10), 1229–1245.
- Gong, Z., Dekkers, M.J., Heslop, D. & Mullender, T.A.T.T. 2009. End-member modelling of isothermal remanent magnetization (IRM) acquisition curves: a novel approach to diagnose remagnetization. *Geophys. J. Int.*, **178**, 693–701.
- Gong, Z., Langereis, C.G. & Mullender, T.A.T. 2008. The rotation of Iberia during the Aptian and the opening of the Bay of Biscay. *Earth planet. Sci. Lett.*, **273**, 80–93.
- Gutiérrez-Alonso, G., López-Carmona, A., Núñez-Guerrero, E., García, A.M., Fernández-Suárez, J., Pastor-Galán, D., Gutiérrez-Marco, J.C. et al. 2020. Neoproterozoic-Palaeozoic detrital sources in the Variscan foreland of northern Iberia: primary vs. recycled sediments, *Geol. Soc., Lond., Spec. Publ.*, **503**, doi:10.1144/SP503-2020-21.
- Gutiérrez-Alonso, Gabriel, Collins, A.S., Fernández-Suárez, J., Pastor-Galán, D., González-Clavijo, E., Jourdan, F., Weil, A.B. et al. 2015. Dating

- of lithospheric buckling: 40Ar/39Ar ages of syn-orocline strike-slip shear zones in northwestern Iberia. *Tectonophysics*, **643**, 44–54.
- Harrison, R.J. & Feinberg, J.M., 2008. FORCinel: An improved algorithm for calculating first-order reversal curve distributions using locally weighted regression smoothing. *Geochemistry, Geophysics, Geosystems*, **9**(1).
- Heslop, D., Dekkers, M.J., Kruiver, P.P. & Van Oorschot, I.H.M. 2002. Analysis of isothermal remanent magnetization acquisition curves using the expectation-maximization algorithm. *Geophys. J. Int.*, **148**, 58–64.
- Heslop, D. & Dillon, M. 2007. Unmixing magnetic remanence curves without a priori knowledge. *Geophys. J. Int.*, **170**, 556–566.
- Heslop, D., McIntosh, G. & Dekkers, M.J. 2004. Using time- and temperature-dependent Preisach models to investigate the limitations of modelling isothermal remanent magnetization acquisition curves with cumulative log Gaussian functions. *Geophys. J. Int.*, **157**, 55–63.
- Hoareau, G., Cognier, N., Lacroix, B., Aubourg, C., Roberts, N. M., Niemi, N. & Ruiz, I. S. 2021. Combination of Δ47 and U-Pb dating in tectonic calcite veins unravel the last pulses related to the Pyrenean Shortening (Spain). *Earth planet. Sci. Lett.*, **553**, 116636.
- Huang, W., Dupont-Nivet, G., Lippert, P.C., Hinsbergen, D.J.J. van, Dekkers, M.J., Guo, Z., Waldrup, R. et al. 2015. Can a primary remanence be retrieved from partially remagnetized Eocene volcanic rocks in the Nanmulin Basin (southern Tibet) to date the India-Asia collision? *J. geophys. Res.*, **120**, 42–66.
- Huang, W., Jackson, M.J., Dekkers, M.J., Solheid, P., Zhang, Y., Li, S., Guo, Z. & Ding, L., 2020. Remagnetization of red beds on the Tibetan Plateau: Mechanism and diagnosis, *Journal of Geophysical Research: Solid Earth*, **125**(8) e2020JB020068.
- Huang, W., Lippert, P.C., Zhang, Y., Jackson, M.J., Dekkers, M.J., Li, J., Hu, X. et al. 2017. Remagnetization of carbonate rocks in southern Tibet: perspectives from rock magnetic and petrographic investigations. *J. geophys. Res.*, **122**, 2434–2456.
- Huyghe, D., Mouthereau, F., Castelltort, S., Filleaudeau, P. Y. & Emmanuel, L. 2009. Paleogene propagation of the southern Pyrenean thrust wedge revealed by finite strain analysis in frontal thrust sheets: implications for mountain building. *Earth planet. Sci. Lett.*, **288**(3–4), 421–433.
- Izquierdo-Llavall, E., Aldega, L., Cantarelli, V., Corrado, S., Gil-Peña, I., Invernizzi, C. & Casas, A. M. 2013. On the origin of cleavage in the Central Pyrenees: structural and paleo-thermal study. *Tectonophysics*, **608**, 303–318.
- Izquierdo-Llavall, E., Casas-Sainz, A. M., Oliva-Urcia, B., Villalaín, J. J., Pueyo, E. & Scholger, R. 2018. Rotational kinematics of basement antiformal stacks: paleomagnetic study of the western Nogueras Zone (Central Pyrenees). *Tectonics*, **37**(10), 3456–3478.
- Izquierdo-Llavall, E., Casas-Sainz, A., Oliva-Urcia, B. & Scholger, R. 2014. Palaeomagnetism and magnetic fabrics of the Late Palaeozoic volcanism in the Castejón-Laspáñoles basin (Central Pyrenees). Implications for palaeoflow directions and basin configuration. *Geol. Mag.*, **151**(5), 777–797.
- Izquierdo-Llavall, E., Menant, A., Aubourg, C., Callot, J. P., Hoareau, G., Camps, P. & Lahfid, A. 2020. Preorogenic folds and syn-orogenic basement tilts in an inverted hyperextended margin: the northern Pyrenees case study, *Tectonics*, **39**(7), e2019TC005719, doi:10.1029/2019TC005719.
- Izquierdo-Llavall, E., Sainz, A. C., Oliva-Urcia, B., Burmester, R., Pueyo, E. L. & Housen, B. 2015. Multi-episodic remagnetization related to deformation in the Pyrenean Internal Sierras. *Geophys. J. Int.*, **201**(2), 891–914.
- Jackson, M., Rochette, P., Fillion, G., Banerjee, S. & Marvin, J. 1993. Rock magnetism of remagnetized Paleozoic carbonates: low-temperature behavior and susceptibility characteristics. *J. geophys. Res.*, **98**, 6217–6225.
- Jolivet, M., Labaume, P., Monié, P., Brunel, M., Arnaud, N. & Campani, M. 2007. Thermochronology constraints for the propagation sequence of the south Pyrenean basement thrust system (France-Spain), *Tectonics*, **26**(5).
- Juárez, M. T., Lowrie, W., Osete, M. L. & Meléndez, G. 1998. Evidence of widespread Cretaceous remagnetisation in the Iberian Range and its relation with the rotation of Iberia. *Earth planet. Sci. Lett.*, **160**(3–4), 729–743.
- Keller, P., Lowrie, W. & Gehring, A. U. 1994. Palaeomagnetic evidence for post-thrusting tectonic rotation in the Southeast Pyrenees, Spain. *Tectonophysics*, **239**(1–4), 29–42.
- Kirschvink, J.L. 1980. The least-squares line and plane and the analysis of palaeomagnetic data. *Geophys. J. Int.*, **62**, 699–718.
- Kleinsmiede, W.F.J. 1960. Geology of the Valle de Arán (Central Pyrenees). *Leidse Geologische Mededelingen*, **25**, 129–245.
- Koymans, M.R., Hinsbergen, D.J.J. van, Pastor-Galán, D., Vaes, B. & Langereis, C.G. 2020. Towards FAIR Paleomagnetic Data Management Through Paleomagnetism.org 2.0. *Geochem. Geophys. Geosyst.*, **21**, e2019GC008838. doi:10.1029/2019GC008838.
- Koymans, M.R.R., Langereis, C.G.G., Pastor-Galán, D. & Hinsbergen, D.J.J.J.D.J.J. van. 2016. Paleomagnetism.org: an online multi-platform open source environment for paleomagnetic data analysis, *Comput. Geosci.*, **93**, 127–137.
- Kruiver, P.P., Dekkers, M.J. & Heslop, D. 2001. Quantification of magnetic coercivity components by the analysis of acquisition curves of isothermal remanent magnetisation. *Earth planet. Sci. Lett.*, **189**, 269–276.
- Kuiper, K.F., Deino, A., Hilgen, F.J., Krijgsman, W., Renne, P.R. & Wijbrans, J.R. 2008. Synchronizing rock clocks of Earth history. *Science*, **320**, 500–504.
- Labaume, P., Meresse, F., Jolivet, M., Teixell, A. & Lahfid, A., 2016. Tectonothermal history of an exhumed thrust-sheet-top basin: An example from the south Pyrenean thrust belt, *Tectonics*, **35**(5), 1280–1313.
- Labaume, P., Séguret, M. & Seyve, C. 1985. Evolution of a turbiditic foreland basin and analogy with an accretionary prism: example of the Eocene south-Pyrenean basin. *Tectonics*, **4**(7), 661–685.
- Labaume, P. & Teixell, A. 2018. 3D structure of subsurface thrusts in the eastern Jaca Basin, southern Pyrenees. *Geologica Acta*, **16**(4), 477–498.
- Labagabrielle, Y., Labaume, P. & de Saint Blanquat, M., 2010. Mantle exhumation, crustal denudation, and gravity tectonics during Cretaceous rifting in the Pyrenean realm (SW Europe): insights from the geological setting of the Iherzolite bodies, *Tectonics*, **29**(4).
- Lanaja, J. M., 1987. Contribución de la exploración petrolífera al conocimiento de la Geología de España. [http://info.igme.es/geologiasub\\_suelo/GeologiaSubsuelo/Documents.aspx](http://info.igme.es/geologiasub_suelo/GeologiaSubsuelo/Documents.aspx). Instituto Geológico y Minero de España Ed., 465, 17 mapas.
- Larraoña, J.C., Parés, J.M., del Valle, J. & Millán, H., 2003. Triassic paleomagnetism from the Western Pyrenees revisited: implications for the Iberian-Eurasian Mesozoic plate boundary, *Tectonophysics*, **362**(1), 161–182.
- Leite Mendes, B.D., Pastor-Galán, D., Dekkers, M.J. & Krijgsman, W. 2021. Avalonia, get bent! – Paleomagnetism from SW Iberia confirms the Greater Cantabrian Orocline. *Geoscience Frontiers*, **12**, 805–825.
- Martínez-Peña, M. & Casas-Sainz, A. 2003. Cretaceous–tertiary tectonic inversion of the Cotiella Basin (southern Pyrenees, Spain). *Int. J. Earth Sci.*, **92**(1), 99–113.
- Maxbauer, D.P., Feinberg, J.M. & Fox, D.L. 2016. MAX UnMix: a web application for unmixing magnetic coercivity distributions. *Comp. Geosci.*, **95**, 140–145.
- McCabe, C. & Elmore, R. D. 1989. The occurrence and origin of late Paleozoic remagnetization in the sedimentary rocks of North America. *Rev. Geophys.*, **27**(4), 471–494.
- McCabe, C., Van der Voo, R., Peacor, D. R., Scotese, C. R. & Freeman, R. 1983. Diagenetic magnetite carries ancient yet secondary remanence in some Paleozoic sedimentary carbonates. *Geology*, **11**(4), 221–223.
- McClelland, E. A. & McCaig, A. M. 1988. Palaeomagnetic estimates of total rotation in basement thrust sheets, Axial Zone, Southern Pyrenees. *Cuadernos de Geología Ibérica*, **12**, 181–193.
- McClelland, E. & McCaig, A. M. 1989. Palaeomagnetic estimates of rotations in compressional regimes and potential discrimination between thin-skinned and deep crustal deformation, in *Paleomagnetic Rotations and Continental Deformation*, NATO ASI Series C, 254, pp. 365–379, eds Kissel, C. & Laj, C., Springer.
- McFadden, P.L.L. & McElhinny, M.W. 1988. The combined analysis of remagnetization circles and direct observations in palaeomagnetism. *Earth planet. Sci. Lett.*, **87**, 161–172.

- Millán-Garrido, H., Oliva-Urcia, B. & Pocoví-Juan, A. 2006. La transversal de Gavarnie-Guara; estructura y edad de los mantos de Gavarnie, Guara-Gedre y Guarga (Pirineo centro-occidental). *Geogaceta*, **40**, 35–38.
- Mochales, T., Casas, A. M., Pueyo, E. L. & Barnolas, A. 2012. Rotational velocity for oblique structures (Boltaña anticline, Southern Pyrenees). *J. Struct. Geol.*, **35**, 2–16.
- Mochales, T., Pueyo, E. L., Casas, A. M. & Barnolas, A. 2016. Restoring paleomagnetic data in complex superposed folding settings: the Boltaña anticline (Southern Pyrenees). *Tectonophysics*, **671**, 281–298.
- Mujal, E., Fortuny, J., Pérez-Cano, J., Dinarès-Turell, J., Ibáñez-Insa, J., Oms, O. & Anadón, P. 2017. Integrated multi-stratigraphic study of the Coll de Terrers late Permian–Early Triassic continental succession from the Catalan Pyrenees (NE Iberian Peninsula): a geologic reference record for equatorial Pangaea. *Global Planet. Change*, **159**, 46–60.
- Mullender, T. A. T., Fredericks, T., Hilgenfeldt, C., de Groot, L. V., Fabian, K. & Dekkers, M. J. 2016. Automated paleomagnetic and rock magnetic data acquisition with an in-line horizontal “2G” system. *Geochem. Geophys. Geosyst.*, **17**, 3546–3559.
- Mullender, T.A.T. Van Velzen, A.J. & Dekkers, M.J. 1993. Continuous drift correction and separate identification of ferrimagnetic and paramagnetic contributions in thermomagnetic runs, *Geophysical Journal International*, **114**(0), 663–672.
- Müller, R.D., Zahirovic, S., Williams, S.E., Cannon, J., Seton, M., Bower, D.J., Tetley, M.G. et al. 2019. A global plate model including lithospheric deformation along major rifts and Orogenes since the Triassic. *Tectonics*, **38**, 1884–1907.
- Muñoz, J. A. 1992. Evolution of a continental collision belt: eCORS-Pyrenees crustal balanced cross-section, in *Thrust Tectonics*, pp. 235–246. Springer.
- Muñoz, J. A. 2019. Alpine Orogeny: deformation and Structure in the Northern Iberian Margin (Pyrenees sl), in *The Geology of Iberia: A Geodynamic Approach*, pp. 433–451, Springer.
- Muñoz, J. A., Beamud, E., Fernández, O., Arbués, P., Dinarès-Turell, J. & Poblet, J. 2013. The Ainsa Fold and thrust oblique zone of the central Pyrenees: kinematics of a curved contractional system from paleomagnetic and structural data. *Tectonics*, **32**(5), 1142–1175.
- Muñoz, J. A., Martínez, A. & Vergés, J. 1986. Thrust sequences in the eastern Spanish Pyrenees. *J. Struct. Geol.*, **8**(3–4), 399–405.
- Muñoz, J. A., Mencos, J., Roca, E., Carrera, N., Gratacós, O., Ferrer, O. & Fernández, Ó. 2018. The structure of the South-Central-Pyrenean fold and thrust belt as constrained by subsurface data. *Geologica Acta*, **16**(4), 439–460.
- Nance, R.D., Gutiérrez-Alonso, G., Keppie, J.D., Linnemann, U., Murphy, J.B., Quesada, C., Strachan, R.A. et al. 2010. Evolution of the Rheic Ocean. *Gondwana Res.*, **17**, 194–222.
- Neres, M., Miranda, J.M. & Font, E. 2013. Testing Iberian kinematics at Jurassic-Cretaceous times. *Tectonics*, **32**, 1312–1319.
- Nirrengarten, M., Manatschal, G., Tugend, J., Kusznir, N. & Sauter, D. 2018. Kinematic evolution of the southern North Atlantic: implications for the formation of hyperextended rift systems. *Tectonics*, **37**(1), 89–118.
- Oliva-Urcia, B., 2018. Thirty years of advances in the knowledge of the structural evolution of the south-central Pyrenees during the Cenozoic collision, a summary, *Revista de la Sociedad Geológica de España*, **31**, 51–68.
- Oliva-Urcia, B., Casas, A. M., Pueyo, E. L., Román-Berdiel, T. & Geissman, J. W. 2010. Paleomagnetic evidence for dextral strike-slip motion in the Pyrenees during alpine convergence (Mauléon basin, France). *Tectonophysics*, **494**(3–4), 165–179.
- Oliva-Urcia, B., Casas-Sainz, A.M., Pueyo Morer, E.L. & Pocovi Juan, A., 2012. Structural and paleomagnetic evidence for non-rotational kinematics of the South Pyrenean Frontal Thrust at the western termination of the External Sierras (southwestern central Pyrenees).
- Oliva-Urcia, B. & Pueyo, E. L. 2007a. Gradient of shortening and vertical-axis rotations in the Southern Pyrenees (Spain), insights from a synthesis of paleomagnetic data. *Revista de la Sociedad Geológica de España*, **20**(1–2), 105–118.
- Oliva-Urcia, B. & Pueyo, E. L. 2007b. Rotational basement kinematics deduced from remagnetized cover rocks (Internal Sierras, southwestern Pyrenees), *Tectonics*, **26**(4),
- Oliva-Urcia, B. & Pueyo, E. L. 2019. Paleomagnetism in structural geology and tectonics, in *Teaching Methodologies in Structural Geology and Tectonics*, pp. 55–121, Springer.
- Oliva-Urcia, B., Pueyo, E. L. & Larrasoña, J. C. 2008. Magnetic reorientation induced by pressure solution: a potential mechanism for orogenic-scale remagnetizations. *Earth planet. Sci. Lett.*, **265**(3–4), 525–534.
- Oliva-Urcia, B., Pueyo, E. L., Larrasoña, J. C., Casas, A. M., Román-Berdiel, T., Van der Voo, R. & Scholger, R. 2012. New and revisited paleomagnetic data from Permian–Triassic red beds: two kinematic domains in the west-central Pyrenees. *Tectonophysics*, **522**, 158–175.
- Oliveira, J.T., Quesada, C., Pereira, Z., Matos, J.X., Solá, A.R., Rosa, D., Albardeiro, L. et al. 2019. South Portuguese Terrane: a continental affinity exotic unit, in *The Geology of Iberia: A Geodynamic Approach*, Regional Geology Reviews, pp. 173–206, eds Quesada, C. & Oliveira, J.T., Springer International Publishing.
- Parés, J.M., 2015. Sixty years of anisotropy of magnetic susceptibility in deformed sedimentary rocks. *Front. Earth Sci.*, **3**, 4.
- Pastor-Galán, D., Ursem, B., Meere, P.A. & Langereis, C. 2015. Extending the Cantabrian Orocline to two continents (from Gondwana to Laurussia). Paleomagnetism from South Ireland, *Earth planet. Sci. Lett.*, **432**, 223–231, doi:10.1016/j.epsl.2015.10.019.
- Pastor-Galán, D., Groenewegen, T., Brouwer, D., Krijgsman, W. & Dekkers, M.J. 2015a. One or two oroclines in the Variscan orogen of Iberia? Implications for Pangea amalgamation. *Geology*, **43**, 527–530.
- Pastor-Galán, Daniel, Dekkers, M.J., Gutiérrez-Alonso, G., Brouwer, D., Groenewegen, T., Krijgsman, W., Fernández-Lozano, J. et al. 2016. Paleomagnetism of the Central Iberian curve’s putative hinge: too many oroclines in the Iberian Variscides. *Gondwana Res.*, **39**, 96–113.
- Pastor-Galán, Daniel, Gutiérrez-Alonso, G., Dekkers, M.J.M.J. & Langereis, C.G.C.G.C.G. 2017. Paleomagnetism in Extremadura (Central Iberian zone, Spain) Paleozoic rocks: extensive remagnetizations and further constraints on the extent of the Cantabrian orocline. *J. Iberian Geol.*, **43**, 583–600.
- Pastor-Galán, Daniel, Gutiérrez-Alonso, G., Murphy, J.B.B., Fernández-Suárez, J., Hofmann, M. & Linnemann, U. 2013. Provenance analysis of the Paleozoic sequences of the northern Gondwana margin in NW Iberia: passive margin to Variscan collision and orocline development. *Gondwana Res.*, **23**, 1089–1103.
- Pastor-Galán, Daniel, Gutiérrez-Alonso, G. & Weil, A.B. 2011. Orocline timing through joint analysis: insights from the Ibero-Armorican Arc. *Tectonophysics*, **507**, 31–46.
- Pastor-Galán, Daniel, Gutiérrez-Alonso, G. & Weil, A.B. 2020. The enigmatic curvature of Central Iberia and its puzzling kinematics. *Solid Earth*, **11**, 1247–1273.
- Pastor-Galán, Daniel, Nance, R.D., Murphy, J.B. & Spencer, C.J. 2019. Supercontinents: myths, mysteries, and milestones. *Geol. Soc., Lond., Spec. Publ.*, **470**, 39–64.
- Pastor-Galán, Daniel, Pueyo, E.L., Diederichs, M., García-Lasanta, C. & Langereis, C.G. 2018. Late Paleozoic Iberian Orocline(s) and the Missing Shortening in the Core of Pangea. Paleomagnetism From the Iberian Range. *Tectonics*, **37**, 3877–3892.
- Pereira, M.F., Castro, A., Chichorro, M., Fernández, C., Díaz-Alvarado, J., Martí, J. & Rodríguez, C. 2014. Chronological link between deep-seated processes in magma chambers and eruptions: permo-Carboniferous magmatism in the core of Pangaea (Southern Pyrenees). *Gondwana Res.*, **25**, 290–308.
- Pérez-Cáceres, I., Martínez Poyatos, D., Simancas, J.F. & Azor, A. 2017. Testing the Avalonian affinity of the South Portuguese Zone and the Neoproterozoic evolution of SW Iberia through detrital zircon populations. *Gondwana Res.*, **42**, 177–192.
- Porquet, M., Pueyo, E. L., Román-Berdiel, T., Olivier, P., Longares, L. A., Cuevas, J. & Auréjac, J. B. 2017. Anisotropy of magnetic susceptibility of the Pyrenean granites. *J. Maps*, **13**(2), 438–448.
- Pueyo, E. L. 2000. Rotaciones paleomagnéticas en sistemas de pliegues y cabalgamientos. Tipos, causas, significado y aplicaciones (ejemplos del

- Pirineo Aragonés). *Unpublished PhD thesis*, Universidad de Zaragoza, 296.
- Pueyo, E. L., Beamud, E., Muñoz, J. A., Rodríguez-Pintó, A. & San Miguel, G. 2016b. Remagnetización alpina en la Serra del Cadí (Pirineo Oriental). *Geo-Temas*, **16**(1), 869–872.
- Pueyo, E. L., García-Lasanta, C., López, M. A., Oliván, C., San Miguel, G., Gil-Garbi, Hthe GeoKin3DPyr working group *et al.* the GeoKin3DPyr working group 2017. Metodología para el desarrollo de la BBDD paleomagnética de Iberia (EPOS-DDSS Iberian Paleomagnetism). In MAG-IBER, X.(pp. 94–99). *Instituto de Investigación en Ciencias Ambientales (IUCa)*. Universidad de Zaragoza. ISBN: 978-84-16723-40-9.
- Pueyo, E. L., Oliva-Urcia, B., Sánchez-Moreno, E.M., Arenas, C., Silvas-Casal, R., Calvín, P., Santolaria, P., García-Lasanta, C., Oliván, C., Gil-Imaz, A., Compairead, F., Casas, A.M. & Pocoví, A. 2021a. The geometry and kinematics of the Southwestern termination of the Pyrenees; a field guide to the Santo Domingo anticline. In *Structural Geology and Tectonics Field Guidebook-* Mukherjee, S. (Editor). Chapter 3, 52pp. Springer. ISBN 978-3-030-60142-3.
- Pueyo, E. L., Sussman, A. J., Oliva-Urcia, B. & Cifelli, F. 2016a. Palaeomagnetism in fold and thrust belts: use with caution. *Geol. Soc., Lond., Spec. Publ.*, **425**(1), 259–276.
- Pueyo, E.L., Mauritsch, H.J., Gawlick, H.J., Scholger, R. & Frisch, W. 2007. New evidence for block and thrust sheet rotations in the central northern Calcareous Alps deduced from two pervasive remagnetization events, *Tectonics*, **26**(5).
- Pueyo, E.L., Rodríguez-Pintó, A., Serra-Kiel, J. & Barnolas, A. 2021b. The chronology and rotational kinematics in the Eastern Jaca Basin (Southern Pyrenees): las Bellotas section, *Geol. Acta*, in press.
- Puigdefábregas, C., 1975. La sedimentación molásica en la cuenca de Jaca. Monografías del instituto de estudios pirenaico, *Número extraordinario de revista de Pirineos. Jaca*.
- Puigdefábregas, C., Muñoz, J. A. & Vergés, J. 1992. Thrusting and foreland basin evolution in the southern Pyrenees, in *Thrust Tectonics*, pp. 247–254, Springer.
- Ramón, M. J., Pueyo, E. L., Oliva-Urcia, B. & Larrasoña, J. C. 2017. Virtual directions in paleomagnetism: a global and rapid approach to evaluate the NRM components, *Front. Earth Sci.*, **5**.
- Ramón, M. J., Pueyo, E. L., Oliva-Urcia, B., Scholger, R., Román-Berdiel, M. T. & Casas, A. M. 2016. Squeezing paleomagnetic information using virtual directions; an example from the Bielsa granite (Axial Pyrenees). *Geotemas*, **16**(1), 873–876.
- Ribeiro, M.L., Reche, J., López-Carmona, A., Aguilar, C., Bento dos Santos, T., Chichorro, M., Dias da Silva, I. *et al.* 2019. *Variscan Metamorphism. in The Geology of Iberia: A Geodynamic Approach*, Regional Geology Reviews, pp. 431–495, eds Quesada, C. & Oliveira, J.T., Springer International Publishing, doi:10.1007/978-3-030-10519-8\_12.
- Robador, A., Samsó, J.M., Ramajo, J., Barnolas, A., Clariana, P. & Martín, S. Gil, I 2019. (2; Mapa Geológico Digital continuo E. 1:50.000, Zona Pirineos Vasco-Cantábrica (Zona-1600). in GEODE. *Mapa Geológico Digital continuo de España*. <http://info.igme.es/cartografiadigital/geologica/geodezona.aspx?id=Z1600>.
- Robardet, M. 2003. The Armorica ‘microplate’: fact or fiction? Critical review of the concept and contradictory palaeobiogeographical data. *Palaeogeog. Palaeoclimat. Palaeoecol.*, **195**, 125–148.
- Rodríguez-Pintó, A., Pueyo, E. L., Calvín, P., Sánchez, E., Ramajo, J., Casas, A. M. & Román, T. 2016. Rotational kinematics of a curved fold: the Balzes anticline (Southern Pyrenees). *Tectonophysics*, **677**, 171–189.
- Rouvier, H., Henry, B. & Le Goff, M. 2012. Mise en évidence par le paléomagnétisme de rotations régionales dans la virgation des Corbières (France). *Bulletin de la Société géologique de France*, **183**(5), 409–424.
- Santolaria, P., Ayala, C., Pueyo, E. L., Rubio, F. M., Soto, R., Calvín, P. & Casas-Sainz, A. M. 2020. Structural and geophysical characterization of the western termination of the South Pyrenean triangle zone. *Tectonics*, **39**(8), e2019TC005891.
- Scheepers, P. J. J. & Zijderveld, J. D. A. 1992. Stacking in Paleomagnetism: application to marine sediments with weak NRM. *Geophys. Res. Lett.*, **19**(14), 1519–1522.
- Schmidt, P. W. 1982. Linearity spectrum analysis of multi-component magnetizations and its application to some igneous rocks from south-eastern Australia. *Geophys. J. Int.*, **70**(3), 647–665.
- Schwarz, E. J. 1963. A paleomagnetic investigation of Permo-Triassic red beds and andesites from the Spanish Pyrenees. *J. geophys. Res.*, **68**(10), 3265–3271.
- Schwarz, E.J. 1974. Magnetic fabric in massive sulfide deposits. *Can. J. Earth Sci.*, **11**, 1669–1675.
- Schwarz, E.J. & Vaughan, D.J. 1972. Magnetic phase relations of Pyrrhotite. *J. Geomag. Geoelectr.*, **24**, 441–458.
- Shaw, J., Johnston, S.T. & Gutiérrez-Alonso, G. 2015. Orocline formation at the core of Pangea: a structural study of the Cantabrian orocline, NW Iberian Massif. *Lithosphere*, **7**, 653–661.
- Sitter, L.U. & Zwart, H.J. 1957. Geological map of the Paleozoic of the Central Pyrenees. *Leidse Geologische Mededelingen*, **22**, 351–418.
- Stampfli, G.M., Hochard, C., Vérard, C., Wilhem, C. & VonRaumer, J. 2013. The Formation of Pangea. *Tectonophysics*, **593**, 1–19.
- Sussman, A. J., Butler, R. F., Dinarès-Turell, J. & Vergés, J. 2004. Vertical-axis rotation of a foreland fold and implications for orogenic curvature: an example from the Southern Pyrenees, Spain. *Earth planet. Sci. Lett.*, **218**(3-4), 435–449.
- Tait, J. 1999. New Early Devonian paleomagnetic data from NW France: paleogeography and implications for the Armorican microplate hypothesis. *J. geophys. Res.*, **104**, 2831–2839.
- Tait, J. A., Bachadse, V. & Dinarès-Turell, J. 2000. Paleomagnetism of Siluro-Devonian sequences, NE Spain. *J. geophys. Res.*, **105**(B10), 23 595–23 603.
- Tait, J., 1999. New Early Devonian paleomagnetic data from NW France: paleogeography and implications for the Armorican microplate hypothesis, *Journal of Geophysical Research: Solid Earth*, **104**(D), 2831–2839.
- Tait, J., Bachadse, V. & Soffel, H. 1994. New palaeomagnetic constraints on the position of central Bohemia during Early Ordovician times. *Geophys. J. Int.*, **116**, 131–140.
- Tauxe, L., 2010. Essentials of paleomagnetism, *University of California Press*.
- Teixell, A. 1996. The Ansó transect of the southern Pyrenees: basement and cover thrust geometries. *J. geol. Soc. Lond.*, **153**(2), 301–310.
- Teixell, A. & Muñoz, J. A. 2000. Evolución tectono-sedimentaria del Pirineo meridional durante el Terciario: una síntesis basada en la transversal del río Noguera Ribagorçana. *Revista de la Sociedad Geológica de España*, **13**, 251–264.
- Torsvik, T.H., Voo, R.V.D., Preeden, U., Mac, C., Steinberger, B., Doubrovine, P.V., Hinsbergen, D.J.J.V. *et al.* 2012. Phanerozoic polar wander, palaeogeography and dynamics. *Earth Sci. Rev.*, **114**, 325–368.
- van der Lingen, G. J. 1960. Geology of the Spanish Pyrenees, north of Canfranc, Huesca province (Doctoral dissertation, Instituto di investigaciones geológicas). *Estudios Geológicos XVI*, 206–242
- Van der Voo, R. 1969. Paleomagnetic evidence for the rotation of the Iberian Peninsula. *Tectonophysics*, **7**(1), 5–56.
- Van der Voo, R. 1993. *Paleomagnetism of the Atlantic, Tethys and Iapetus oceans*. Cambridge Univ. Press.
- Van der Voo, R. & Torsvik, T. H. 2012. The history of remagnetization of sedimentary rocks: deceptions, developments and discoveries. *Geol. Soc., Lond., Spec. Publ.*, **371**(1), 23–53.
- Van Dongen, P. G. 1967. The rotation of Spain: palaeomagnetic evidence from the eastern Pyrenees. *Palaeogeog. Palaeoclimat. Palaeoecol.*, **3**, 417–432.
- van Velzen, A.J. & Zijderveld, J.D.A. 1995. Effects of weathering on single-domain magnetite in Early Pliocene marine marls. *Geophys. J. Int.*, **121**, 267–278.
- Villalain, J. J., Casas-Sainz, A. M. & Soto, R. 2016. Reconstruction of inverted sedimentary basins from syn-tectonic remagnetizations. A methodological proposal. *Geological Society, London, Special Publications*, **425**(1), 233–246.
- Vine, F.J. & Matthews, D.H. 1963. Magnetic anomalies over oceanic ridges. *Nature*, **199**, 947–949.

- Vissers, R.L.M. & Meijer, P.Th. 2012. Mesozoic rotation of Iberia: subduction in the Pyrenees? *Earth Sci. Rev.*, **110**, 93–110.
- Waldner, M. 2019. *Cinématique et thermicité du prisme orogénique des Pyrénées : nouvelles données géo-thermochronologiques de la Zone Axiale*. Sciences de la Terre. Sorbonne Université, 2019.
- Weil, A. B., Gutiérrez-Alonso, G. & Conan, J. 2010. New time constraints on lithospheric-scale oroclinal bending of the Ibero-Armorican Arc: a palaeomagnetic study of earliest Permian rocks from Iberia. *J. geol. Soc. Lond.*, **167**, 127–143.
- Weil, A. B., Voo, R. van der & Pluijm, B.A. van der. 2001. Oroclinal bending and evidence against the Pangea megashear: the Cantabria-Asturias arc (northern Spain). *Geology*, **29**, 991–994.
- Weil, Arlo Brandon, Gutiérrez-Alonso, G. & Wicks, D. 2013. Investigating the kinematics of local thrust sheet rotation in the limb of an orocline: a paleomagnetic and structural analysis of the Esla tectonic unit, Cantabrian–Asturian Arc, NW Iberia. *Int. J. Earth Sci. (Geol Rundsch.)*, **102**, 43–60.
- Weltje, G.J. 1997. End-member modeling of compositional data: numerical-statistical algorithms for solving the explicit mixing problem. *Math. Geol.*, **29**, 503–549.
- Zijderveld, J. D. A. 1967. AC demagnetization of rocks: analysis of results, in *Methods in Paleomagnetism*, eds Collinson, D.W., Creer, K.M. & Runcorn, S.K., Elsevier.
- Zwart, H.J., 1979. The geology of the Central Pyrenees.
- Zwart, H.J., 1986. The Variscan geology of the Pyrenees, *Tectonophysics*, **129**(1–4) 9–27.

## SUPPORTING INFORMATION

Supplementary data are available at [GJI](#) online.

SF1: All thermomagnetic curves analysed.

SF2: All Hysteresis loops analysed.

SF3: (a) Synthesis of the palaeomagnetic results (can be opened with palaeomagnetism.org). (b) Extra plots and table showing the mean VRM per site and the mean ChRM per site in tectonic coordinates.

SF4: KMZ file (Google Earth) with the sampled locations.

SF5: Graphics showing all results of the AMS analyses.

SF6: Zip file containing all obtained raw results.